High and low permeability of human pluripotent stem cell–derived blood–brain barrier models depend on epithelial or endothelial features

Stéphane D Girard, Ingrid Julien-Gau, Yves Molino, Benjamin F Combes, Louise Greetham, Michel Khrestchatisky, Emmanuel Nivet

Received: 31 August 2022 | Revised: 21 December 2022 | Accepted: 28 December 2022

DOI: 10.1096/fj.202201422R

THE FASEB JOURNAL

RESEARCH ARTICLE

High and low permeability of human pluripotent stem cell–derived blood–brain barrier models depend on epithelial or endothelial features

Stéphane D. Girard[1,2] | **Ingrid Julien-Gau**[2] | **Yves Molino**[2] | **Benjamin F. Combes**[2] | **Louise Greetham**[1] | **Michel Khrestchatisky**[1] | **Emmanuel Nivet**[1]

[1]Institute of NeuroPhysiopathology, INP, CNRS, Aix-Marseille University, Marseille, France

[2]Faculty of Medicine, VECT-HORUS SAS, Marseille, France

Correspondence
Michel Khrestchatisky and Emmanuel Nivet, Institute of NeuroPhysiopathology, INP, CNRS, Aix-Marseille University, Marseille, France.
Email: michel.khrestchatisky@univ-amu.fr and emmanuel.nivet@univ-amu.fr

Funding information
Agence Nationale de la Recherche (ANR), Grant/Award Number: ANR-15-CE18-0010 and ANR-17-EURE-0029; Aix-Marseille Université, Grant/Award Number: AMX-19-IET-004

Abstract

The search for reliable human blood–brain barrier (BBB) models represents a challenge for the development/testing of strategies aiming to enhance brain delivery of drugs. Human-induced pluripotent stem cells (hiPSCs) have raised hopes in the development of predictive BBB models. Differentiating strategies are thus required to generate endothelial cells (ECs), a major component of the BBB. Several hiPSC-based protocols have reported the generation of in vitro models with significant differences in barrier properties. We studied in depth the properties of iPSCs byproducts from two protocols that have been established to yield these in vitro barrier models. Our analysis/study reveals that iPSCs derivatives endowed with EC features yield high permeability models while the cells that exhibit outstanding barrier properties show principally epithelial cell-like (EpC) features. We found that models containing EpC-like cells express tight junction proteins, transporters/efflux pumps and display a high functional tightness with very low permeability, which are features commonly shared between BBB and epithelial barriers. Our study demonstrates that hiPSC-based BBB models need extensive characterization beforehand and that a reliable human BBB model containing EC-like cells and displaying low permeability is still needed.

KEYWORDS

blood–brain barrier modeling, endothelial differentiation, epithelial cells, human brain microvascular endothelial cells, human-induced pluripotent stem cells

Abbreviations: Ac-LDL, acetylated low-density lipoprotein; BBB, blood-brain barrier; bFGF, basic fibroblast growth factor; BMP4, bone morphogenic protein 4; BMVEC, brain microvascular endothelial cells; BSA, bovine serum albumin; CNS, central nervous system; CspA, cyclosporin A; EC, endothelial cell; ECEM, endothelial cell expansion medium; ECIM, endothelial cell induction medium; ECM, extracelullar matrix; EpC, epithelial cell; FPKM, fragment per kilobase million; GSK3β, glycogen synthase kinase 3 beta; HBMVECs, human brain microvascular endothelial cells; hiPSCs, human-induced pluripotent stem cells; HUVECs, human umbilical vein endothelial cells; LY, lucifer yellow; MACS, magnetic activated cell sorting; NVU, neurovascular unit; Pe, permeability; Pr-1, protocol 1; PSCs, pluripotent stem cells; RA, retinoic acid; RPKM, read per kilobase million; TEER, trans-endothelial electrical resistance; TGFβ, transforming growth factor beta; TNF-α, tumor necrosis factor-alpha; UM, unconditioned medium; VEGF, vascular endothelial growth factor.

1 | INTRODUCTION

Blood vessels that vascularize the central nervous system (CNS) possess unique properties and are collectively referred to as the blood–brain barrier (BBB). The BBB is composed of specialized brain microvascular endothelial cells (BMVECs) that establish intercellular tight junctions, surrounded by pericytes, astrocytes, and neurons, altogether forming the neurovascular unit (NVU). CNS vessels are non-fenestrated and BMVECs tightly regulate CNS homeostasis, notably the movement of ions, molecules, and cells between the blood and the brain.[1] These properties rely in part on the expression of BBB-specific receptors, transporters, and efflux pumps at the level of BMVECs. Interactions of BMVECs with other cells of the NVU precisely control the brain microenvironment and protect the CNS from toxic compounds, pathogens, inflammation, injury, and disease.[2,3] BBB dysfunctions and inflammation accompany neurodegenerative disorders indicating that it plays a key role in these disorders.[4] If the highly selective permeability of the BBB is essential to preserve CNS integrity from a large variety of putative toxic products, it also represents a major obstacle to deliver pharmaco-active compounds to the brain.[5]

Accordingly, the use of robust in vitro BBB models recapitulating at least in part phenotypical and functional characteristics is of major relevance to study BBB physiopathology as well as to predict the cerebral exposure of new neuro-pharmaceuticals.[6] In vitro BBB models produced from animal brain microvessels have been widely used for studying the BBB but they have limitations impacting their predictability such as limited tightness, batch to batch variabilities, phenotypic alterations during isolation and culture as well as inter-species differences.[7,8] Thus, the establishment of predictive and robust human cell-based BBB models is still required to address interspecies differences at the molecular, cellular, and functional levels. Until recently, modeling of the human BBB was restricted to the use of human primary BMVECs or to immortalized human cell lines, both presenting limitations for drug screening and trans-endothelial transport evaluation. For instance, primary human BMVECs are usually obtained from *post-mortem* tissue or patient biopsies and have obvious limitations regarding availability, scalability, and reproducibility. Besides, BBB-like models generated from human endothelial cell (EC) lines have failed to show optimal barrier properties.[2,7] Of interest, BMVECs and epithelial cells share key features that are important for functional barriers. This includes the expression of tight junction proteins, the expression of transporters/efflux pumps as well as high junctional tightness.[9,10] Accordingly, another strategy developed to model functional barrier-like properties has been to use epithelial cell (EpC) lines such as human intestinal Caco-2 cells as surrogate BBB models.[9] However, the disparity in the expression of transporter genes between BBB and these EpCs limit their predictability as BBB models.[8,10–12]

Recently, new promising strategies based on the use of other cellular sources such as human cord blood-derived hematopoietic stem cells or endothelial progenitors have been proposed to produce brain-like ECs.[13,14] Concomitantly, the use of human-induced pluripotent stem cells (hiPSCs) has gained large interest as starting material for alternative strategies.[15–17] Indeed, in addition to their human origin, these cells present several advantages including virtually unlimited cell source (scalability) and the potential to differentiate into any cell type (versatility) and, in the BBB context, to generate the different cellular components of the NVU.[18] Moreover, hiPSCs are easily available and can be produced from patient cells to study genetic diseases and potentially BBB dysfunctions associated with specific diseases/mutations.[19,20]

A prerequisite for using hiPSCs as BBB modeling tools is the development of efficient protocols to direct their differentiation into functional BMVECs. On the one hand, several studies, based on chemically defined methods, have described the conversion of pluripotent stem cells (PSCs) into ECs with variable efficiencies.[21–31] These procedures are based on the use of small molecules and growth factors activating key signaling pathways aiming to recapitulate the early developmental stages of EC generation. Similar differentiation paradigms, based on three main steps, are generally described: a mesodermal induction followed by an endothelial/vascular induction that precedes an EC expansion phase coupled with a cell sorting procedure to obtain nearly pure EC populations. However, to our knowledge, attempts to specify those PSC-derived ECs into BMVEC-like cells have not yet been fully satisfactory and these cells show insufficient barrier properties.[15,32,33]

On the other hand, Lippmann and collaborators demonstrated the possibility to obtain cells with exceptional barrier properties from human PSCs using a fundamentally different procedure.[34] This strategy, which was subsequently improved[35–40] and adapted by many different groups,[41–49] is based on an undirected/spontaneous differentiation process assumed to promote neural and endothelial co-differentiation. These cells have also been used in complex microfluidic systems[50–56] and combined with other NVU cells derived from the same hiPSC lines to produce human BBB models.[57–59] The generation of patient-derived cells using this undirected method to study BBB dysfunction in neurological disorders has also been reported.[60–63] However, the phenotype of the cells generated according to this protocol has been a subject of controversy[64] as some recent studies have reported conflicting data regarding the vascular/endothelial identity of these cells,[55,65,66] which

could be EpCs misidentified as BMVECs.[67] In the search of identifying the best available strategy to establish a reliable human BBB modeling platform for further applications, we performed a thorough analysis of the cellular phenotype and barrier properties generated by undirected/spontaneous differentiation of hiPSCs.[34,35] Our results were compared with the cellular phenotype and barrier properties of hiPSC derivatives obtained with an alternative protocol based on a chemically defined mesodermal induction. This other protocol was described to efficiently generate EC-like cells without specific brain endothelial features.[23] Our study confirms that chemically defined mesodermal induction of hiPSCs generated cells with endothelial-like features, but rather poor barrier properties. In contrast, undirected/spontaneous differentiation of hiPSCs yielded exquisite barrier properties but with cells that presented essentially an epithelial-like phenotype.

2 | MATERIAL AND METHODS

2.1 | Cell culture

Three human iPSC lines were used as previously characterized: KiPS 4F2,[68] BJIPS 6F,[69] and iPS (IMR90)-4[70] (Table S1). Human iPSCs (hiPSCs) were cultured in a chemically defined growth medium (StemMACS iPS-Brew XF (Miltenyi Biotec) or mTSeR™1 (Stem Cell Technologies)) on plates coated with growth factor reduced matrigel (8.7 μg/cm^2, Corning). For passaging, 70%–80% confluent iPSCs were treated with a cell dissociation buffer (0.5 mM EDTA, 1.8 mg/ml NaCl, D-PBS without Ca^{2+}/Mg^{2+}) for 3 min at RT, and colonies were dispersed to small clusters using a 5-ml glass pipette and carefully replated at a splitting ratio of about 1:4. Expression of PSC transcription factors (Nanog, Oct3/4, and Sox2) by the three human iPSC lines was controlled by flow cytometry, using BD Stemflow Human Pluripotent Stem Cell Transcription Factor Analysis Kit® (BD Biosciences) according to the manufacturer's instructions. Human umbilical vein endothelial cells (HUVECs) were cultured in EBM-2 medium supplemented with EGM-2 SingleQuots (Lonza) on plates coated with rat tail collagen I (20 μg/cm^2, Corning). Human brain microvascular endothelial cells (HBMVECs) were cultured in Endothelial Growth Medium (EGM, Angio-proteomie, PELOBiotech) on plates coated with human fibronectin (10 μg/ml, Corning). The hCMEC/D3 cells were cultured in EBM-2 medium supplemented with EGM-2 MV SingleQuots (Lonza) on plates coated with rat tail collagen I (20 μg/cm^2, Corning). For RT-qPCR experiments, hCMEC/D3 cells grown at confluence were differentiated for 5 days in the same medium but without the growth factors. Caco-2 and human skin fibroblast cells were grown in Dulbecco's modified Eagles medium (DMEM) with Glutamax (Life Technologies) and supplemented with 10% fetal bovine serum, 100 units/ml of penicillin and 100 μg/ml of streptomycin (Life Technologies). All cell types were maintained at 37°C in a humidified incubator at 5% CO2 with medium changes every day (hiPSCs) or every second day for the other cell types.

2.2 | Differentiation of hiPSCs into Ecs

2.2.1 | Protocol 1 (Pr-1)

This differentiation procedure is based on the protocol reported by Patsch et al.[23,71] with slight modifications. In short, hiPSCs at 70%–80% of confluence were dissociated with StemPro Accutase (Life technologies) and singularized cells were seeded at a defined density (between 42 000 and 62 000 cells/cm^2 depending on the hiPSC line) on matrigel coated 6-well plates in StemMACS iPS-Brew supplemented with 10 μM Y27632 (ROCK inhibitor, Tocris Bioscience). After 24 h (Figure 1), the medium was replaced with Priming Medium (1:1 mixture of DMEM/F12 with Glutamax and Neurobasal media, supplemented with 1x N2 and B27 (Life Technologies), 8 μM CHIR99021 (Tocris Bioscience), 25 μg/ml human recombinant Bone Morphogenetic Protein 4 (BMP4, R&D Systems) and 55 μM β-mercaptoethanol (Life technologies)). After 3 days in the medium, it was replaced for 2 days by EC Induction Medium (ECIM: StemPro-34 SFM medium, Life Technologies) supplemented with 200 ng/ml human recombinant Vascular Endothelial Growth Factor (VEGF165, PeproTech) and 2 μM forskolin (Sigma-Aldrich). The ECIM was renewed the following day. On day five ECs were dissociated with StemPro Accutase (diluted 1:6 in D-PBS) and separated via Magnetic-activated cell sorting (MACS, Miltenyi Biotec) using CD34 MicroBeads, LS Columns and MidiMACS Separator according to the manufacturer's protocol. CD34-positive cells were replated on dishes coated with 10 μg/ml human fibronectin (Corning) at a density of 1×10^5 cells/cm^2 in EC Expansion Medium (ECEM: StemPro-34 SFM with 100 ng/ml VEGF). ECEM was replaced every other day. Once confluence was reached (usually 3 days), the cells were either cryopreserved or directly seeded in ECEM (with 50 ng/ml VEGF) medium at a cell density of 0.5×10^6 cells/cm^2 on microporous (1 μm) polyethylene membrane (12- or 6-well insert filters, Greiner Bio-One) to establish EC monolayers or at a density of 0.25×10^6 cells/cm^2 on tissue culture-treated plates for other experiments. Filters and plates were coated (24 h, 37°C) with a mixture of collagen type IV and fibronectin (10 μg/ml for both,

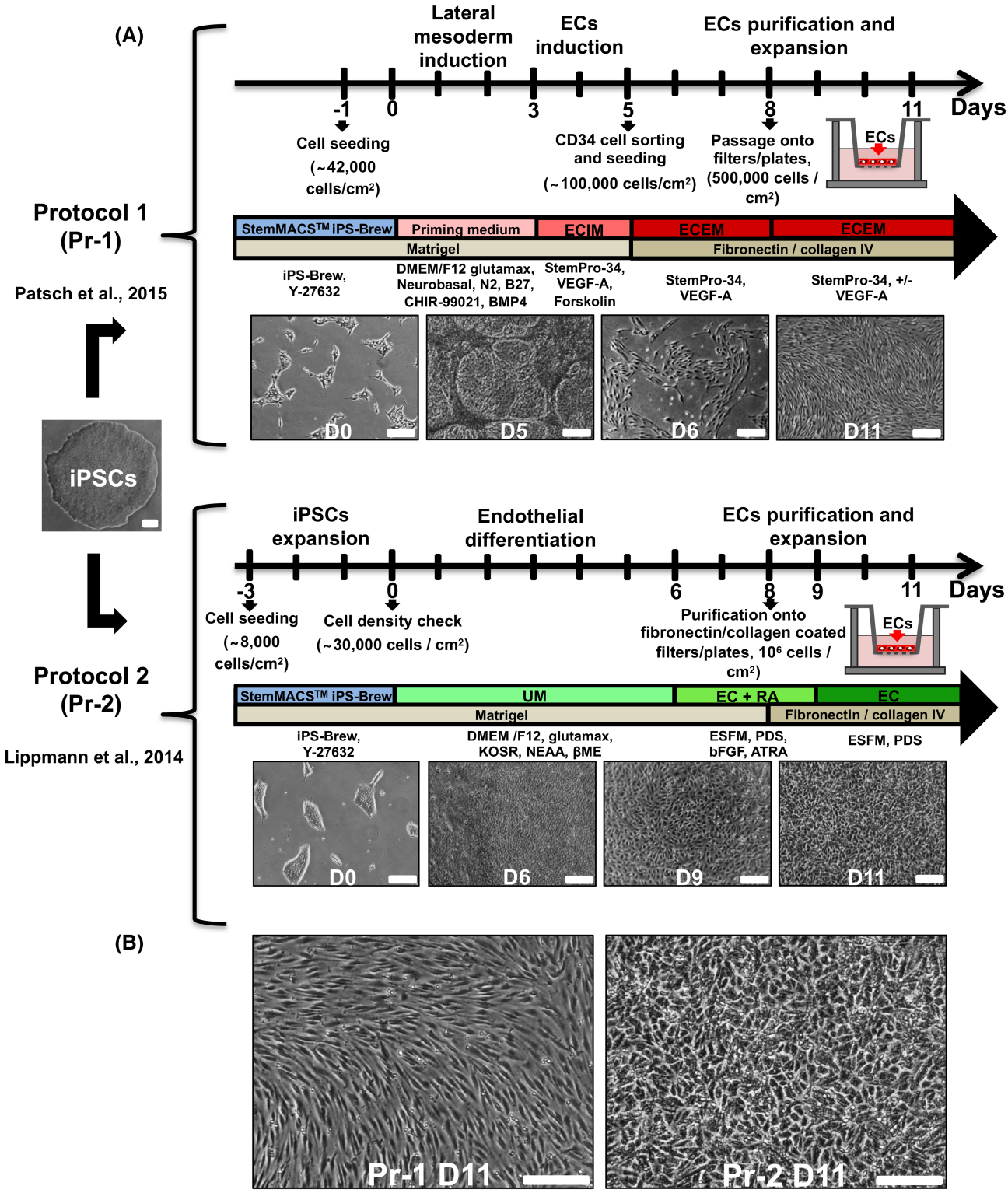

FIGURE 1 Representative overview of the two hiPSCs-based differentiation protocols used in this study. (A) Timelines summarizing the different steps of the two differentiation protocols used throughout the study, namely Pr-1 (top, adapted from Patsch et al. 2015[23]) and Pr-2 (bottom, adapted from Lippmann et al., 2014[35]). A summary of the main components of the different culture media and coatings used at each step of the protocols is indicated and representative bright-field micrographs illustrate the morphology of the cells at different differentiation stages where D stands for Days of differentiation. (B) Higher magnification micrographs corresponding to cells representative of cell population obtained upon completion of the two differentiation protocols and seeded on filters, at day 11 (D11). Scale bars, 0.2 mm (A and B).

Corning) as we previously published for rat brain microvascular cells.[72] The next day, the medium was changed with ECEM (with or without 50 ng/ml of VEGF) and then changed every other day.

2.2.2 | Protocol 2 (Pr-2)

This differentiation procedure is based on the protocol reported by Lippmann et al[34–36,73] HiPSCs grown at 70%–80% of confluence were dissociated with StemPro Accutase and singularized cells were seeded at a defined density (between 7500 and 15 000 cells/cm^2 depending on the hiPSC line) on Matrigel-coated 6-well plates in StemMACS iPS-Brew or mTSeR™1 media supplemented for the first 24 h with 10 μM Y27632 (Figure 1). Three days later, once the cells had reached an optimal cell density of about $3\times10^4\pm5\times10^3$ cells/cm^2, differentiation was initiated, and the medium was changed to an "unconditioned medium" for 6 days with daily changes (UM: DMEM/F-12 ± glutamax, 20% KnockOut Serum Replacement, 1x non-essential amino acids and 0.1 mM β-mercaptoethanol [Life technologies]). On day six, UM was changed for 2 days to an EC medium supplemented with retinoic acid (EC ± RA: human Endothelial-SFM (Life Technologies), 1% platelet-poor plasma-derived bovine serum (Alfa Aesar), 20 ng/ml human recombinant basic fibroblast growth factor (bFGF, PeproTech) and 10 μM all-trans retinoic acid (Sigma-Aldrich)). On day eight, cells were passaged using StemPro Accutase (about 30 min at 37°C) and then either cryopreserved[37] or directly subcultured in EC-RA medium at a cell density of 1×10^6 cells/cm^2 on the microporous membrane to establish EC monolayers (see Pr-1) or at a density of 0.5×10^6 cells/cm^2 on culture-treated polystyrene plates for other experiments. Filters and plates were precoated (24 h, 37°C) with a mixture of 400 μg/ml of collagen type IV and 100 μg/ml of fibronectin (Corning) as previously reported by Lippmann et al.[35] or with the same mixture at 10 μg/ml.[72] The next day the medium was changed with EC medium without bFGF and retinoic acid, and then changed every other day.

2.3 | Flow cytometry analysis

Cells were washed twice in D-PBS and then harvested using StemPro Accutase. Cells were then centrifuged (300 × g, 5 min) and washed once with cold-blocking solution (10% FBS in D-PBS). Expression of EC surface markers (CD31, CD34, and CD144) was performed on living cells. Cells were incubated with the corresponding antibodies or appropriate isotype controls (Table S2) in cold-blocking solution for 1 h on ice in the absence of light. After incubation, cells were washed thrice with cold blocking solution and resuspended in a total volume of 200 μl before analysis. Acquisitions were performed on a FACSCanto II flow cytometer (BD Biosciences) using BDFACSDiva software. At least 10 000 events were recorded for each analysis, and measures were performed in duplicate. Percentages of cells or mean fluorescence intensity are presented after the subtraction of the isotype background and refer to the total population analyzed. Results are representative of at least three independent experiments with a minimum of two technical replicates per experiment.

To exclude bias due to potential enzymatic cleavages of the proteins of interest (surface antigens, EC, or EpC markers) during the cell detachment procedure, the same enzymatic solution (same duration and same concentration) was applied to the different cell types for comparative purposes.

2.4 | Immunocytochemistry and fluorescence microscopy

Cells grown on filters were washed thrice with D-PBS and fixed in 4% paraformaldehyde (PFA, Antigenfix, MM France) for 15 min. Filters with the monolayers were gently dissociated from the plastic inserts with a razor blade before immunocytochemistry. Cells were then blocked and permeabilized for 30 min at RT in blocking buffer that contained 3% bovine serum albumin (BSA) and 0.1% Triton X-100 (Sigma Aldrich). Subsequently, cells were incubated for 90 min at RT with the indicated primary antibody (Table S2) diluted in PBS with 3% BSA. Cells were then washed thrice with PBS and incubated for 1 h RT with the appropriate secondary antibodies and Hoechst 33342 (1 μg/ml Sigma-Aldrich). Cells were washed thrice with PBS, and membranes were mounted in Prolong Gold antifade mounting medium (Thermo Fisher Scientific). Negative control conditions were carried out by omitting the primary antibody. Images were acquired and processed using a confocal microscope (LSM 700) and Zen software (Carl Zeiss).

2.5 | Acetylated low-density lipoprotein uptake assay

For fluorescence microscopy experiments, cells grown at confluence on filters were incubated with 10 μg/ml Alexa Fluor™ 488 acetylated low-density lipoprotein (Ac-LDL) (Thermo Fisher Scientific) in DMEM/F-12 supplemented with 1% BSA for 4 h at 37°C. The cells were washed thrice with PBS and nuclei counterstained with Hoechst 33342

before uptake assessment using confocal microscopy. For flow cytometry analysis, the cells grown at confluence on 24-well plates were incubated with 1 μg/ml Alexa Fluor™ 488 Ac-LDL for 30 min at 37°C. The cells were washed thrice with D-PBS, dissociated using TrypLE Select (Life Technologies), and analyzed by flow cytometry.

2.6 | Vascular tube formation assay

Briefly, 96-well culture plates were coated with 50 μl/well of growth factor reduced matrigel (undiluted, about 1.25 mg/cm^2) for 1 h at 37°C. Cells were dissociated using StemPro Accutase and 100 μl of a cell suspension was dispensed in each well in their respective culture media supplemented with 50 ng/ml VEGF. For each cell type, different cell densities were tested (from 20×10^3 to 140×10^3 cells/cm^2). Tube formation was observed and imaged after 24 h of incubation.

2.7 | RNA isolation and real-time quantitative PCR analysis

Total RNA was isolated using the RNeasy Plus Micro Kit (Qiagen) according to the manufacturer's recommendations. RNA concentration and purity were determined using a NanoDrop-1000 Spectrophotometer (NanoDrop Technologies, Thermo Fisher Scientific). According to the manufacturer's protocol (Thermo Fisher Scientific), 0.5 μg of total RNA was submitted to reverse transcription using Moloney Murine Leukemia Virus reverse transcriptase to generate single-strand cDNA. RT-qPCR experiments were performed with the 7500 Fast Real-Time PCR System (Applied Biosystems/Life Technologies). All reactions were performed using primers listed in the Table S3 and the iTaq Universal SYBR Green Supermix (Bio-Rad Laboratories). Relative expression levels were determined according to the ΔΔCt method with the human housekeeping gene *ABELSON* as endogenous control for normalization as previously described.[74] For each condition, RNA extractions were performed from three independent cultures and the reported values are the mean fold change relative to the value of the control sample (undifferentiated cell line).

2.8 | Trans-endothelial electrical resistance assay

Trans-endothelial electrical resistance (TEER) measurements were performed using a Millicell-ERS (Millipore) volt-ohmmeter connected to an EndOhm chamber (World Precision Instruments) suited for 12-well inserts. TEER measurements were performed in a culture medium 24 h after cell seeding on filters and every 24 h until completion of the kinetic experiment (i.e., 10 days), according to the manufacturer's recommendations. The resistance value (Ω.cm^2) of an empty filter coated with collagen/fibronectin was used as blanks and subtracted from each measurement. All TEER measurements were performed in triplicates (at least three inserts per condition). TEER measurements were also performed on cell monolayers treated with Tumor Necrosis Factor-α (TNF-α). In this case, both the upper and lower compartments were treated with 200 ng/ml TNF-α (PeproTech), and TEER measurements were performed 24 h later and every 24 h for 10 days. TNF-α treatment was renewed every other day.

2.9 | Permeability experiments

The monolayer tightness in 12-well inserts was also assessed by measuring lucifer yellow (LY) (CH dilithium salt, Sigma-Aldrich) permeability as previously described.[72] Briefly, LY was incubated in the upper compartment of the culture system in contact with ECs for 60 min at 37°C in culture medium. Quantification of the LY paracellular leakage was assessed by fluorimetric analysis (excitation at 430 nm and emission at 535 nm) and expressed in LY permeability, Pe (LY).

The in vitro permeability of three substances, Digoxin, Verapamil, and caffeine (Sigma-Aldrich, resuspended in DMSO), was assessed across the EC monolayers. Briefly, these three compounds were incubated at 4 μM in a culture medium for 240 min at 37°C in the upper compartment of HTS 96-well Transwell inserts (Corning). The monolayer integrity was controlled using LY at the end of the experiment. The concentrations of the molecules in samples from upper and lower compartments were quantified using a validated liquid chromatography with tandem mass spectrometry (LC/MS–MS) method at Eurofins/ADME Bioanalyses (Vergeze, France). For each molecule, 12 inserts were quantified. Permeability (Pe) was calculated for each drug as previously described for LY.[72]

2.10 | Functional assay for P-glycoprotein

P-GP efflux activity was assessed by analyzing the intracellular accumulation of rhodamine 123 (R123), a P-GP substrate incubated with or without the addition of the P-GP inhibitor cyclosporin A (CspA). Briefly, the cells grown at confluence on 24-well plates were pre-incubated

with inhibitor at (1, 10, or 50 μM) or with vehicle (DMSO, Dimethyl sulfoxide) in DMEM/F-12 supplemented with 1% BSA for 30 min at 37°C. Then the cells were incubated with R123 (0.1, 0.5, or 1 μM) with or without inhibitor in the same medium for 1 h at 37°C. The cells were then washed once in the culture medium and incubated for 90 min at 37°C with or without an inhibitor. The cells were washed thrice with D-PBS, dissociated using TrypLE Select, and analyzed by flow cytometry. Duplicate samples were measured. Assays were performed at least three times.

2.11 | Statistics

All data are presented as mean ± SEM of at least three independent differentiations/cultures as indicated in the figure captions. Values were compared using Student's *t*-test. The minimal threshold for significance was set at $p \leq .05$.

3 | RESULTS

3.1 | The undirected hiPSC-based differentiation protocol produces cells lacking expression of critical EC markers

To seek the best method able to reproducibly generate hiPSC-derivatives suitable for BBB modeling, we first characterized differentiated cells from three independent hiPSC lines (see Table S1) by comparing two published protocols (Figure 1A). The first protocol (hereafter referred to as Pr-1) was based on a 5-day induction phase with a chemically defined method followed by cell sorting to purify ECs prior to expansion.[23,71] Noteworthy, this protocol was not originally described to promote the generation of ECs with BMVEC-like specifications. The second protocol (hereafter referred to as Pr-2) relied on an 8-day non-chemically defined differentiating method (i.e., resembling embryoid bodies spontaneous differentiating protocols) and further cell purification by sub-culturing them onto a collagen IV/fibronectin matrix.[35,73] By day 11 post-differentiation, both strategies led to the generation of cells that formed a uniform monolayer after seeding at a defined density on a collagen IV/fibronectin-coated membrane (Figure 1B). However, the differentiated cells exhibited significant morphological differences (Figure 1B). Cells obtained with Pr-1 showed a typical elongated spindle-shaped morphology while cells derived with Pr-2 displayed cobblestone-like morphology. Of note, as recommended by Pr-1, the cells were initially expanded in a culture medium containing VEGF, which is an important angiogenic factor well known to induce BBB disruption and, consequently, not compatible with BBB modeling. Thus, for further experiments, we decided to remove VEGF after seeding onto filters. Nevertheless, we noticed that the cell monolayer obtained with Pr-1 derivatives was strongly disorganized upon VEGF removal (Figure S1). To bypass this issue, we established a specific seeding density (0.5×10^6 cells/cm^2) accompanied by a gradual decrease of the VEGF concentration in the culture media that allowed maintaining the organization of the cell monolayer obtained with Pr-1 (Figure 1B).

The strong morphological differences obtained with the two protocols led us to question whether the cells generated from Pr-1 and Pr-2 shared similar expression of EC markers. We first assessed the expression of three cell surface markers, namely CD31/PECAM1, CD34, and CD144/VE-cadherin. For both protocols, the dynamic expression of these EC markers was assessed by flow cytometry at different stages of the differentiation: undifferentiated state (i.e., hiPSC stage or day 0), before sorting or purification (day 5 or 8) and after expansion of the sorted/purified cells (day 11). HUVECs (peripheral ECs) and primary human BMVECs (HBMVECs) were used as positive controls for EC markers while the Caco-2 cell line, representative of epithelial cells (EpCs), was used as negative control (Figure S2). On all three independent hiPSC lines we tested, Pr-1 led to a high yield of differentiating cells displaying a strong expression of all three markers, even before purification (Figure 2A,B and Figure S3A). Thus, before sorting, a high percentage of hiPS derivative obtained from Pr-1 were found positive for CD31 (77.5 ± 7.4%) and CD34 (94.3 ± 2%). After cell sorting, nearly pure populations of cells expressing CD31, CD34, and CD144 were isolated by day 11. Surprisingly, differentiated cells generated with Pr-2 showed no CD31 expression before and after purification while 97.5 ± 0.1% of the primary HBMVECs were positive for this major endothelial marker (Figure 2A,B and Figure S3A). Furthermore, CD34 expression level in the Pr-2 differentiated cells was significantly lower compared with all three undifferentiated hiPSC lines (Figure 2A,B). To assess whether the extracellular matrix (ECM) could impact the differentiation efficacy, we tested two different ECM concentrations of collagen type IV/fibronectin: (i) a mixture of 10 μg/ml of both collagen type IV and fibronectin, according to our own expertise using primary rat BMECs[72] (Mixt. 1) and (ii) a mixture of 400 μg/ml of collagen type IV and 100 μg/ml of fibronectin, based on the Pr-2 recommendation (Mixt.2). In both situations, the Pr-2 protocol failed to generate CD31+ and CD34+ cells (Figure S3B). We next ruled out that the absence of CD31+ cells upon Pr-2-based differentiation was due to the anti-CD31 antibody we used as two distinct antibodies were tested and showed similar

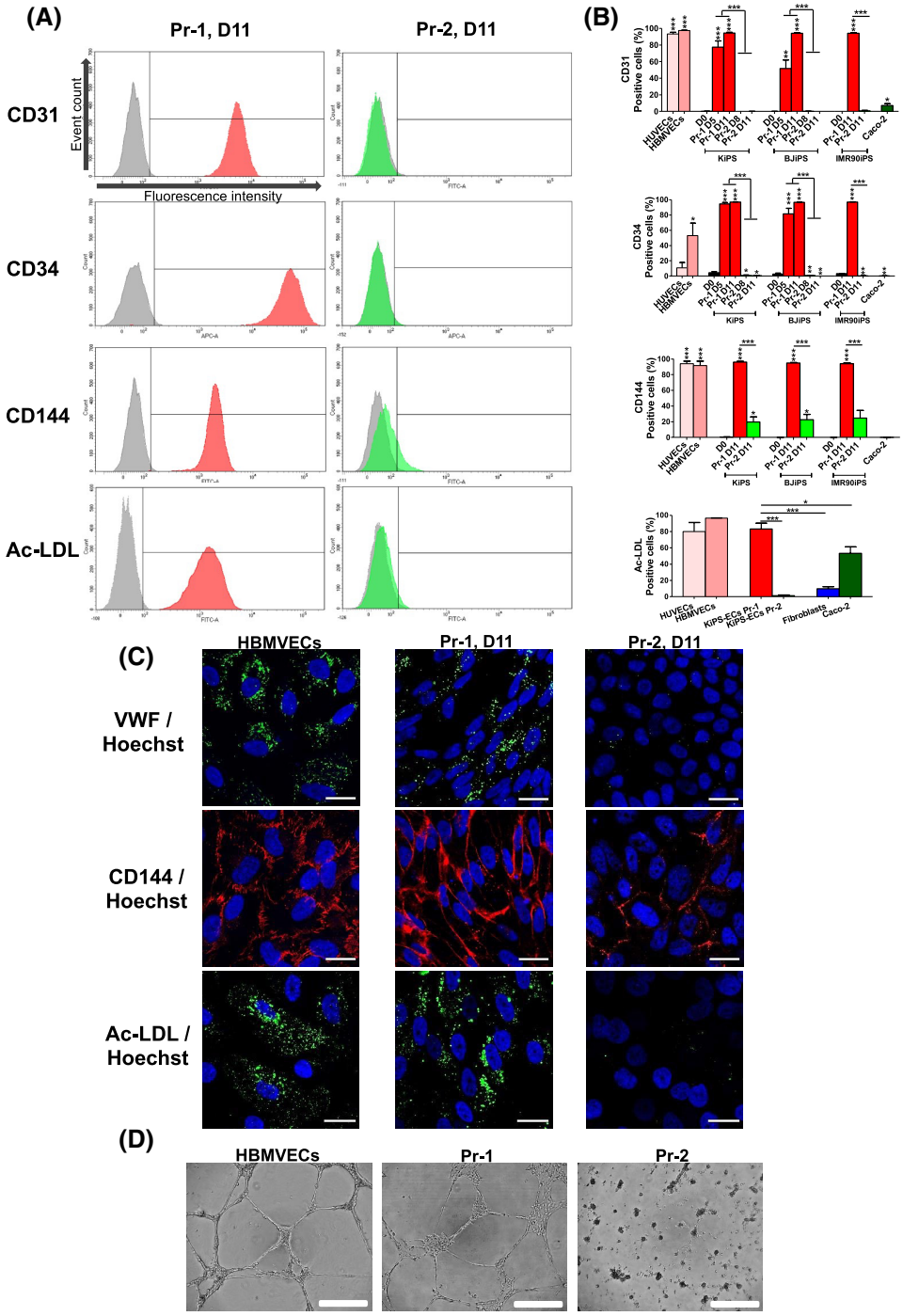

FIGURE 2 Pr-2-derived cells fail to express classical hallmarks of ECs. (A) Representative flow cytometry results showing fluorescence intensity of stained cells in comparison with appropriate isotype controls (gray) in differentiated cells according to Pr-1 (red) and Pr-2 (green) protocols at day 11 (D11). The analyses revealed the absence of classical EC surface markers (as indicated) in Pr-2-derived cells, contrary to Pr-1-derived cells. Pr-2-derivatives were also found unable to uptake fluorescent acetylated LDL (Ac-LDL). (B) Quantification of the percentage of positive cells for the different EC markers and Ac-LDL in hiPSC-derived cells (three independent hiPSC lines) at different stages of the two protocols (D5 and D11) and in cells used as positive (HUVECs and HBMVEC) and negative (Caco-2) endothelial controls. Values reported are the mean (± SEM) of at least three independent differentiations/cultures with $*p \leq .05$, $**p \leq .01$, and $***p \leq .001$, using Student's *t*-test (if not specified, comparison with respective D0 undifferentiated control). (C) Representative fluorescent micrographs showing immunostainings of EC markers including VWF (green, top row), CD144 (red, middle row), and acetylated LDL (green, bottom row). Nuclei were counterstained with Hoechst (blue). (D) Representative bright-field micrographs of the indicated cells 24 h after Matrigel capillary-like tube formation assay. Scale bars: 20 μm (C) and 500 μm (D).

results (Figure S3C). Moreover, we also tested whether the media used to maintain and amplify hiPSCs could impact on the fate of those undifferentiated cells upon differentiating conditions. Thus, we tested the Pr-2 protocol on hiPSCs maintained in either mTeSR™1 or iPS-BREW, and no difference was observed, confirming that the Pr-2 protocol did not generate CD31+ cells and produced very low numbers of CD34+ cells (Figure S3D). Noteworthy, out of the three EC markers we preselected and analyzed, only CD144 was induced by Pr-2, compared with undifferentiated hiPSCs (Figure 2A,B). Moreover, after the purification procedure, 33% of CD144 ± cells were obtained with the Pr-2 protocol at most. These results were further confirmed by immunocytochemistry analyses that revealed a weak and highly heterogeneous CD144 signal at the intercellular junctions of Pr-2-derived cells in comparison with Pr-1 cells and HBMVECs (Figure 2C). Similar differences were also observed with the Von Willebrand Factor (VWF), another EC marker that was strongly expressed within Pr-1-derived cells and HBMVECs and poorly detected in Pr-2-derived cells. Based on these observations, we next decided to deepen the characterization of the Pr-2-derived cells by assessing their functional ability to uptake fluorescent acetylated LDL, a characteristic of ECs.[75] Flow cytometry analyses revealed that sorted CD34+ Pr-1-derived cells were able to uptake Alexa 488 Ac-LDL, similarly to HUVECs and HBMVECs, while purified Pr-2-derived cells displayed a very weak signal, as for fibroblasts that were used as negative control (Figure 2A–C). A matrigel capillary-like tube formation assay was additionally performed, confirming that only cells generated with Pr-1 were able to form tube-like structures, similar to vascular cells such as HBMVEC or HUVECs (Figure 2D and Figure S3E). Of note, we confirmed that the inability of Pr-2-derived cells to generate HBMVEC-like tubes was not due to cell viability prior to seeding (Figure S3E).

Our observations led us to question whether the cells generated by Pr-2 expressed other EC markers or whether their previously described[35] remarkable barrier properties were related to an epithelial phenotype. We thus analyzed by RT-qPCR the gene expression levels of a defined set of 9 EC markers (*PECAM1*, *CD34*, *CDH5*, *VWF*, *ENG*, *FLT1*, *KDR*, *TIE1*, and *TEK*) and 4 EpC markers (*CDH1*, *EPCAM*, *KRT8*, and *CLDN4*) and compared these expression levels with those of ECs (HUVECs, HBMVECs, and HCMEC/D3) and EpCs (Caco-2) used as controls. Confirming our protein expression data, we observed that EC markers were strongly induced in CD34+ Pr-1-derived cells compared with their undifferentiated counterparts (Figure 3A and Figure S4). The gene expression profile of all 9 markers analyzed from Pr-1-derived cells was similar in HUVECs, HBMVECs, and HCMEC/D3, further confirming their EC-like identity. In contrast, purified Pr-2-derived cells expressed EC markers at low or similar levels compared with undifferentiated hiPSCs, with the exception of *CDH5*/*CD144* as previously observed at the protein level. Noteworthy, our analyses also revealed that the expression of the 4 EpC markers in Pr-2-derived cells (Figure 3B) was similar to that of undifferentiated hiPSCs and resembled the Caco-2 gene expression profile. Conversely, these 4 EpC markers were under-expressed in Pr-1-derived cells, HUVECs, HBMVECs, and HCMEC/D3 in comparison with Caco-2 (Figure 3B). For all genes analyzed (Figure 3A,B), significant differences were observed between cells obtained with the two protocols ($p \leq .05$).

It is not likely that our observations result from differences between the cell lines used in our study and those of Lippmann and colleagues, considering that we included in our study the IMR90-4 hiPSC line, which was originally used to set up Pr-2.[34,35] Altogether, our results suggested that cells generated by Pr-2 failed to express typical EC markers, at both transcriptomic and proteomic levels. Moreover, these Pr-2-derived cells lacked critical EC features such as capillary tube formation. Taken together, our data suggest that Pr-1 and Pr-2 generate cells with EC- and EpC-like phenotypes, respectively.

3.2 | Pr-2-derived cells display an EpC-like phenotype

We further questioned whether our observations resulted from in-house experimental bias or from Pr-2. To this end, we leveraged on transcriptomic data sets generated by other groups using Pr-2 and compared them with our gene expression analyzes. We extracted RNA sequencing data (RNA-Seq) from the Gene Expression Omnibus (GEO) database. We selected two groups of genes (24 EC and 10 EpC genes) and directly reported the values uploaded by different authors on the database. We started by analyzing the data previously generated from HBMVECs and purified IMR90-4iPS-derived cells[39] according to a "Pr-2-like" protocol (UM-BMVEC) and to a variant procedure (D-BMVEC2) described by the authors as a more chemically defined method allowing the production of brain ECs in a directed manner (GEO accession number GSE97575). Our analyses revealed that HBMVECs and "Pr-2-like" cells derived from hiPSCs displayed highly different gene expression profiles (Figure 3C). HBMVECs expressed all EC and EpC genes at high and low levels, respectively, compared with UM-BMVEC and D-BMVEC2. Noticeably, critical EC markers such as *PECAM1*, *CD34*, and *CLDN5* displayed zero or near-zero fragment per kilobase million (FPKM) values in "Pr-2-like" cells. Importantly, the D-BMVEC2 cells derived from the "chemically defined

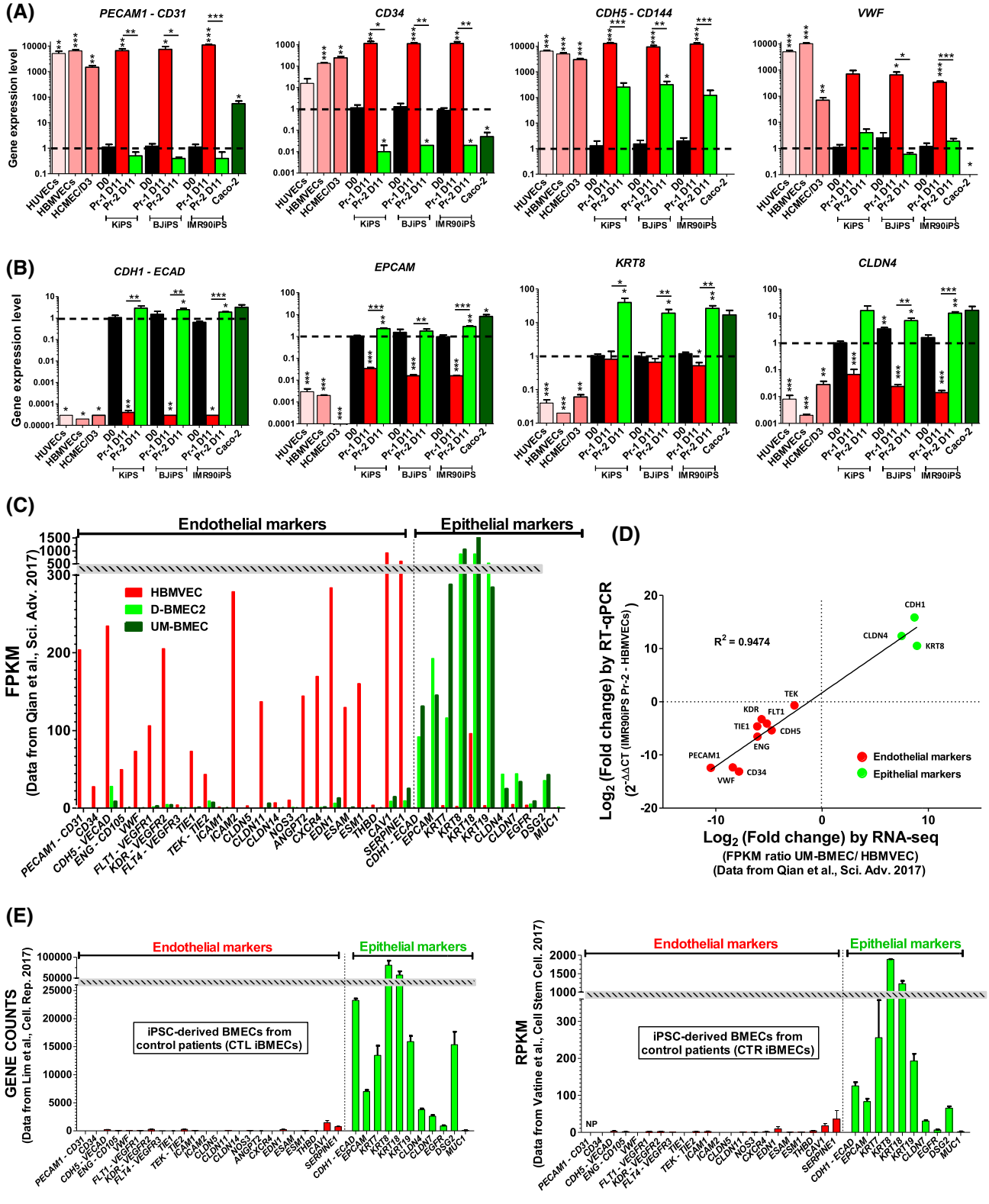

method" exhibited the same gene expression profile. We also compared the fold change values (Pr-2-derived cells vs. HBMVECs) obtained from our RT-qPCR study (Figure 3A,B) with those obtained by RNA-seq reported by Qian and collaborators[39] and showed a high correlation as indicated by the linear regression analysis (r^2 = 0.9474; Figure S5D). Furthermore, we also found these same expression profiles—that is, EC and EpC—from RNAseq data available from four other studies based on "Pr-2-like" protocols (Figure 3E and Figure S5C). In all cases, the reported data indicated a lack or a very low expression of EC genes in comparison with EpC genes (GEO accession numbers: GSE97100,[60] GSE97324,[61] GSE108012,[62] and GSE129290[55]). To

FIGURE 3 Transcriptomic analyses revealed that Pr-2-derived cells display an epithelial-like phenotype. Bar graphs showing the mRNA expression profile of a defined set of EC markers (A) and EpC markers (B) assessed by RT-qPCR in hiPSC-derived cells at different stages of the two protocols. EC (HUVECs, HBMVECs, HCMEC/D3) and EpC (Caco-2) cells were used as positive controls. Values reported are shown as a fold change relative to the value of undifferentiated iPSCs (D0) and are represented as a mean (± SEM) of at least three independent differentiations/cultures with $*p \leq .05$, $**p \leq .01$, and $***p \leq .001$, using Student's *t*-test. (C) Bar graphs showing the gene expression profile of two sets of cell markers representative of endothelial or epithelial cells, respectively. Gene expression levels were from RNAseq analyses obtained by a previous study[39] in HBMVECs and D10 IMR90iPS-derived cells differentiated according to a "Pr-2-like" protocol (UM-BMEC) or to a chemically defined method (D-BMEC2). Values reported are FPKM extracted from the GEO database (accession number GSE97575). (D) Correlative analysis between the relative gene expression of the selected set of genes as measured in the present study by RT-qPCR and the previous study by RNAseq.[39] The value represents the log2 of the fold change between HBMVECs and IMR90iPS-derived ECs differentiated according to the Pr-2 protocol (RT-qPCR) or a "Pr-2-like" protocol (UM-BMEC, RNAseq). (E) Two additional examples of RNAseq data extracted from the GEO database showing the gene expression profiles of EC and EpC markers in other hiPSC-derived ECs differentiated according to a "Pr-2-like" protocols (Left, raw read count abundance; Right, reads per kilobase million (RPKM) accession numbers: GSE97100[60] and GSE97324[61]). NP: not published.

support our findings, we also compared these results with other data sets from RNAseq studies performed in human nasal and intestinal EpCs (GEO accession numbers: GSE 107898[76] and GSE94935[77]). Here again, we found an expression profile comparable with Pr-2-derived cells (Figure S5B) unlike that we observed in other ECs (Figure S5A) such as HUVECs and mouse brain microvascular ECs (GEO accession numbers: GSE93511[78] and GSE111839[79]).

Finally, we performed a further comparison of the Pr-1- and Pr-2-derived cells by studying the expression of EpC protein markers using flow cytometry analyses. We showed that only Pr-1-derived cells lose the expression of Ep-CAM and E-cadherin across the differentiation process, whereas Pr-2-derived cells strongly expressed these two epithelial markers throughout differentiation at levels similar to those of Caco-2 cells (Figure S6A,B). Complementary immunocytochemical analyses against cytokeratin-8 and cytokeratin-18, two other epithelial markers, confirmed their strong expression in undifferentiated hiPSC, Pr-2-derived cells and Caco-2 cells, whereas these markers were barely detectable in Pr-1-derived cells (Figure S6C). Altogether, analyses at the transcriptomic and protein levels provide further evidence indicating that Pr-2-derived cells display an epithelial- rather than endothelial-like phenotype.

3.3 | Pr-2-derived cells express BBB-specific markers

Pr-2-derived cells have been largely used for BBB modeling and we next sought to deepen their characterization. We first analyzed the gene expression levels of a pool of eight BBB markers including three tight junction-related genes (*TJP1-ZO1*, *CLDN5*, *OCLN*) and five genes coding for BBB transporters, receptors, and efflux pumps (*ABCB1-PGP*, *SLC2A1-GLUT1*, *TFRC*, *LDLR*, *SLC7A5-LAT1*). As above, CD34-sorted Pr-1-derived cells and purified Pr-2-derived cells were compared with undifferentiated hiPSCs, peripheral and brain ECs (HUVECs, HBMVECs, and HCMEC/D3) as well as to epithelial cells (Caco-2). For most of the selected genes, significant differences ($p \leq .05$) between Pr-1- and Pr-2-derived cells were found with greater expression of BBB markers in Pr-2-derived cells. This was true for essential BBB genes such as *OCLN*, *PGP*, and *GLUT1*, with the exception of *CLDN5* which was found strongly overexpressed in Pr-1 cells and other ECs but nearly absent in Pr-2-derived cells (Figure 4A).

We also assessed the expression of three classical markers for tight junctions (Z0-1, Claudin-5, and Occludin) by immunolabeling of cell monolayers obtained either with Pr-1, Pr-2, or primary HBMVECs (Figure 4B). Although ZO-1 expression was clearly detectable at the intercellular junctions in all three monolayers, significant differences were observed for Claudin-5 and Occludin. Claudin-5 expression was heterogeneously distributed at the junctions between Pr-1-derived cells, appeared disorganized in Pr-2-derived monolayers and was barely detectable in cultures obtained with primary HBMVECs. Interestingly, the pattern of organization of the Claudin-5 immunodetected in Pr-2-derived cells was similar to the one observed in undifferentiated hiPSCs (Figure 4B and Figure S7A), suggesting no major changes/specifications related to Claudin-5. Noteworthy, our results show discrepancies between mRNA expression levels and protein detection of CLDN-5 in Pr-2-derived cells and HBMVECs. To rule out unspecific binding of the antibody on other claudins, we tested it on the Caco-2 epithelial cell line that strongly expresses several claudins, but not Claudin-5 (or at low levels, as shown in Figure 4A). Our data show that CLDN-5 is barely detectable in Caco-2 cells (Figure S7B), suggesting that the antibody is specific for CLDN-5.

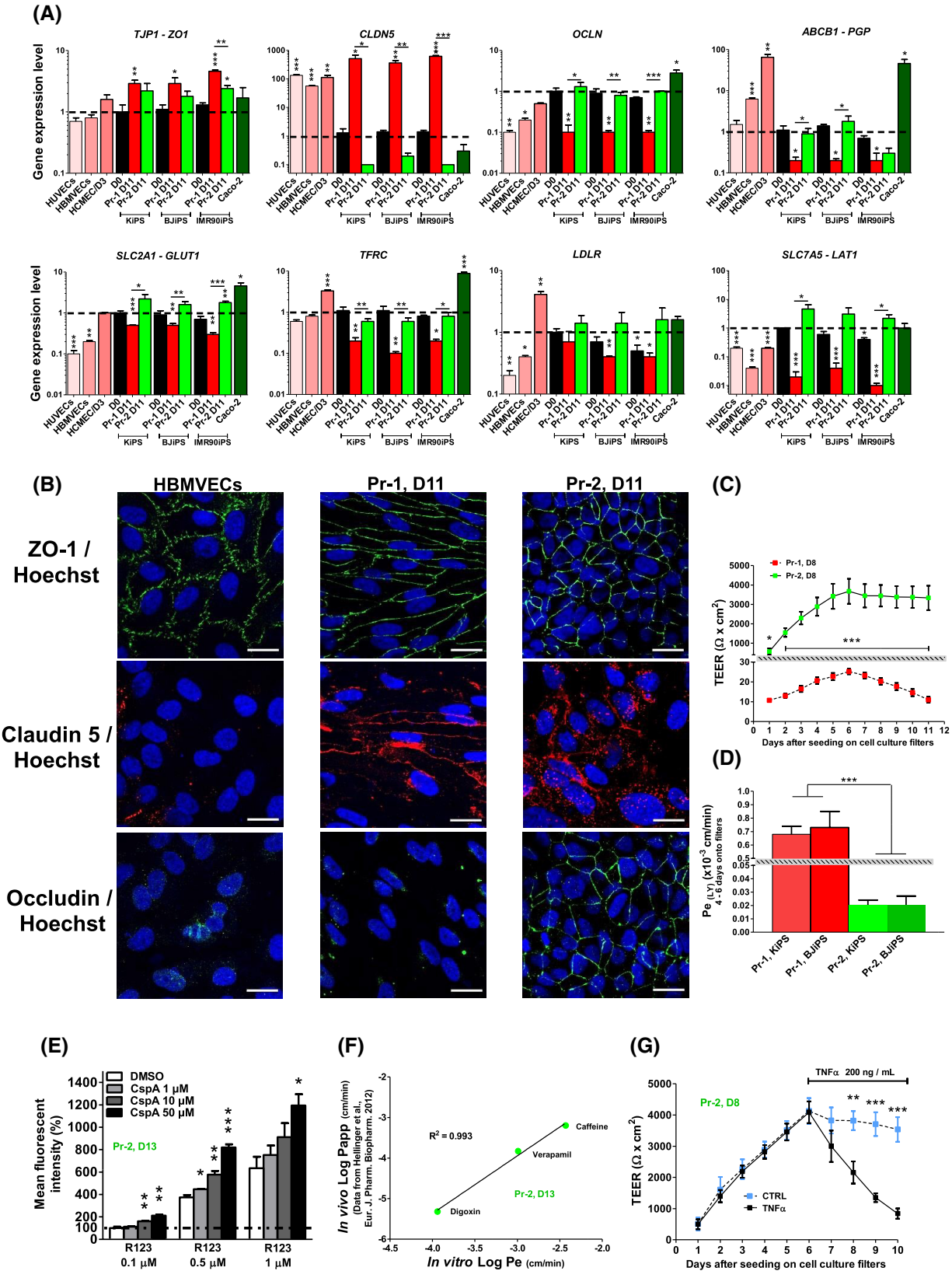

Occludin was only detectable at the intercellular junctions in Pr-2-derived monolayer cultures. Altogether, our observations indicated that Pr-2-derived cells better recapitulated the expression of BBB markers readily related to barrier tightness compared with Pr-1-derived cells and primary HBMVECs.

FIGURE 4 Evaluation of blood–brain barrier (BBB) markers and barrier properties from Pr-1- and Pr-2-derived cells. (A) Bar graphs showing the mRNA expression profile of the indicated BBB markers as assessed by RT-qPCR in human-induced pluripotent stem cell (hiPSC)-derived cells at day 11 of differentiation with either Pr-1 or Pr-2. Endothelial cells (ECs) (HUVECs, HBMVECs, HCMEC/D3) and EpC (Caco-2) were used as controls. Values reported are shown as fold change relative to the value of undifferentiated hiPSCs (D0) and are displayed as a mean (± SEM). (B) Representative fluorescent micrographs showing immunostainings against tight junction proteins including ZO-1 (green, top row), Claudin 5 (red, middle row), and Occludin (green, bottom row). Nuclei were counterstained with Hoechst (blue). (C) Graph showing the kinetics of TEER results in Pr-1 and Pr-2-derived KiPS cells for 11 days after seeding as monolayers on filters at D8 of differentiation. (D) The paracellular permeability to lucifer yellow (LY) was assessed from Pr-1 and Pr-2-derived KiPS and BJiPS cells 4 to 6 days after seeding on filters at D8 of differentiation. Results obtained from cells derived from two independent hiPSC lines are shown. (E) P-glycoprotein (P-GP) efflux activity was measured by intracellular accumulation of Rhodamine 123 (R123) using flow cytometry in the absence (DMSO, vehicle) or presence of the P-GP specific inhibitor cyclosporin A (CspA) in Pr-2-derived cells. (F) Correlation between in vitro permeability coefficients (Pe, x-axis) obtained in KiPS-derived Pr-2 ECs cultured as monolayers and the in vivo apparent permeability coefficients (Papp) previously measured in mice brains[9] of three different drugs as indicated. (G) Graph showing the kinetics of TEER in Pr-2 derivatives in the presence or absence of TNF-α and showing that TNF-α treatment altered the functional integrity of the barrier properties. For all experiments, the values reported are representative of at least three independent differentiations/cultures with $^{*}p \leq .05$, $^{**}p \leq .01$, and $^{***}p \leq .001$ using Student's *t*-test. Scale bars: 20 μm.

3.4 | Pr-2-derived cells display strong barriers properties

Based on our observations, we then performed analyses at the functional level to evaluate the tightness of the above-mentioned cell monolayers by assessing the TEER and the paracellular permeability to LY (Figure 4C,D). After cell seeding on the top of a microporous membrane classically used for BBB modeling, we performed a dynamic analysis for 11 days of the TEER of cultures derived from sorted Pr-1-derived cells and purified Pr-2-derived cells, which revealed strong significant differences from the very first day ($p \leq .001$). After 5 days of seeding, Pr-2-derived cells reached a very high TEER value ($3676.5 \pm 644\,\Omega.cm^2$) that lasted for at least 7 days, whereas the TEER values obtained with the Pr-1 cells remained below $30\,\Omega.cm^2$ (Figure 4C). Similarly, significant differences were obtained when we analyzed LY permeability (Figure 4D). After 5 days on filters Pr-1-derived cells reached a mean Pe (LY) of $0.7 \times 10^{-3} \pm 0.1$ cm/min, while Pr-2-derived cells exhibited a mean Pe (LY) of $0.02 \times 10^{-3} \pm 0.007$ cm/min after ($p \leq .001$). Of note, it has been previously reported that TEER values of about $150–200\,\Omega.cm^2$ are the lowest functional limit for in vitro models,[6,80] but such values may not necessarily reflect the BBB permeability and are likely to depend on the nature of the compounds being transported. Moreover, in vivo BBB TEER is estimated at much higher values ranging from 1500 to $8000\,\Omega.cm^2$.[8] Consequently, in view of the low tightness measured with Pr-1-derived cells that we could not optimize, we only pursued the functional characterization of the Pr-2-derived cells. We used flow cytometry analysis to measure the functionality of the P-glycoprotein (P-GP) efflux pump by assessing the intracellular accumulation of Rhodamine 123 (R123), a cell-permeable P-GP substrate, in the absence or presence of cyclosporin A (CspA), a P-GP specific inhibitor (Figure 4E). We observed a dose-dependent effect of the inhibitor demonstrated by an increase of the R123 accumulation in purified Pr-2-derived cells, which started to be significant at 1 μM of CspA with 0.5 μM of R123 ($p \leq .05$) compared with the vehicle control. We observed a 2.05-fold increase (±0.1) in R123 cellular accumulation in the presence of 50 μM CspA. In addition, we assessed the in vitro permeability (Pe) through Pr-2-derived cell monolayers of three small molecules (Digoxin, Verapamil, and Caffeine) known to display different, in vivo brain penetration because of their different size, lipophilicity, and ability to bind to efflux transporters.[9] The in vitro Pe values of these molecules measured by LC/MS–MS and in vivo apparent permeability coefficients (Papp) previously measured in mice brains[9] showed a very high correlation as indicated by the linear regression analysis ($r^2 = 0.993$) (Figure 4F). We completed the characterization of the Pr-2-derived monolayers by analyzing the effect of a pro-inflammatory cytokine (TNFα) on their integrity (Figure 4G). The TEER kinetic study indicated a strong decrease in the tightness of cytokine-treated monolayers, which started to be significant after 48 h of treatment ($p \leq .001$). Overall, different functional assays confirmed that Pr-2-derived cells displayed strong barrier properties.

4 | DISCUSSION

Human iPSCs have enormous potential for the development of human in vitro models that can provide new platforms for fundamental research but also screening/testing/validation of molecules in the context of preclinical studies on humanized systems. As a prerequisite, such models need to closely recapitulate both phenotypic and functional features of the tissue(s) or cell type(s) to be studied. In this perspective, establishing a reliable and scalable human BBB model is paramount for the study of active molecules on the human BBB, their ability not only

to cross this physical barrier but also to develop strategies to deliver molecules that cannot naturally pass the BBB. Considering that BMVECs represent one of the key components of the BBB, one major challenge for BBB modeling is the generation of hiPSC-derived ECs displaying a cerebral phenotype and that reproduce in vitro the landmarks of the BBB in vivo.

4.1 | Pr-2-derived cells show good barrier properties but limited endothelial features

In 2012, the Shusta laboratory[34] reported an efficient method to produce human cells endowed with characteristics of the in vivo BBB. The cells produced with this method, which was subsequently improved in a series of follow-up reports,[35,39,73] have been originally described as ECs exhibiting good barrier properties. Especially, an outstanding tightness has been reported with very high TEER values rising up to 8000 Ω.cm^2.[59] These TEER values exceed by far those usually observed with in vitro BBB models based on primary BMVECs or BMVEC lines.[6,7,81] Such high values were close to estimates reported for the BBB electrical resistance in vivo[8] (from few hundreds up to 6000–8000 Ω.cm^2) and promoted the interest of Pr-2-derived cells for BBB modeling. This protocol could provide a highly potent alternative to other in vitro BBB models displaying high TEER values but which are based on epithelial cells, such as Caco-2 or MDCK cells,[8,81] and so lacking the necessary endothelial features associated with the BBB in physiological conditions. The Pr-2 protocol is relatively simple as it does not require multiple steps involving the application of well-defined titers of small molecules and growth factors known to activate key developmental signaling pathways, which is usually the strategy followed to differentiate PSCs into ECs.[21,23,25] Indeed, during the first 6 days of this differentiation procedure, small hiPSC colonies solely require DMEM and knock-out serum, indicating that removal of factors that maintain the pluripotent state of hiPSCs, is sufficient to produce differentiated cells efficiently. The only molecules added to the differentiation medium the next 3 days (day 6 to day 9) are bFGF in the first report[34] and, according to the following reports, all-trans retinoic acid that significantly improved the barrier properties.[35] Moreover, this method involves purification of cells by a sub-culture onto collagen IV/fibronectin matrix and does not require cell sorting procedures based on endothelial surface markers (such as CD31, CD34, or CD144), as usually performed to obtain nearly pure EC populations from PSCs.[21–23,25] The Shusta group reported that its procedure is based on PSCs co-differentiation into both neural and endothelial lineages providing an "embryonic brain-like microenvironment" allowing the specification of ECs into BMVECs via a Wnt/β-catenin signaling.[34] Although it is well accepted that the embryonic brain environment is key for BMVECs specification, the latter have a mesodermal origin distinct from the neuro-ectodermal neural cells and acquire their BBB properties only after migrating into the developing brain from the perineural vascular plexus.[82–84] Most studies describing the generation of ECs from PSCs include a defined mesodermal induction step based on the use of specific molecules such as glycogen synthase kinase 3 β (GSK3β) inhibitors, BMP4 or Activin A. This mesoderm induction step is usually combined with activators of the endothelial phenotype such as VEGF, cyclic AMP activators, or inhibitors of transforming growth factor beta (TGFβ) signaling.[21–27,32] In the present study, we compared cells obtained in the absence of such a mesodermal-induction step (Pr-2) with cells produced with a fully defined procedure (Pr-1). Our results showed that Pr-2 promotes the generation of epithelial-like cells rather than ECs, as demonstrated by the critical lack of induction for several key endothelial markers. Indeed, among the top-most essential endothelial markers—that is, CD31/PECAM-1, CD34, CD144/CDH5/VE-cadherin and VWF, CD105/ENG, VEGFR1/FLT1, VEGFR2/KDR, TIE1, TIE2/TEK, CLDN5—only VE-cadherin was induced by Pr-2, both at the transcriptomic and proteomic levels. Although our data are strongly correlated with transcriptomic data published by different groups with this same protocol, some differences exist, at the protein level, when compared with some data from the literature. This is especially the case for CD31/PECAM-1, Claudin-5, and, to a lesser extent, CD144/VE-cadherin. Regarding CD31/PECAM-1, our data showed neither mRNA induction nor protein expression, which is in agreement with recent results from Lu et al[64,67] However, such results are also contradictory with those reported by Lippmann et al. and other groups who originally described PECAM-1 expression on iPSC differentiation with this protocol.[34,41,43,46,85] Nevertheless, it must be noted that transcriptomic data from this same group showed the lack of expression or an extremely low expression of this canonical endothelial marker,[39,55,60,62] thus highlighting some discrepancies in the original report. To rule out any iPSC line-specific effects or technical issues, we used the same detection antibody and the same iPSCs line as originally reported but, once again, the Pr-2 protocol failed to generate iPSC derivatives expressing PECAM-1. Similarly, and regarding CD144/VE-cadherin, although we observed a slight induction of this marker at both transcriptomic and proteomic levels, our data revealed a much lower expression than originally reported.[35,85] Of note, others

reported the absence of CD144 expression,[64,65,67] which is more in line with our observations. In the case of VE-cadherin, it is important to indicate that different detection antibodies were used by the different groups, which could be one of the possible explanations for these conflicting results. Another difference relates to Claudin-5, which is a key tight junction protein also considered as a pan-endothelial marker at the transcriptional level.[86] As for PECAM-1, our gene expression data showed very low CLDN5 mRNA levels in Pr-2-derived cells, which was in agreement with other transcriptomic data generated from Pr-2-derived cells.[39,55,60–62,67] Intriguingly, we noticed a very poor correlation between the mRNA levels and the detection of CLDN-5 in Pr-2-derived cells and HBMVECs. For HBMVECs; one possible explanation for this discrepancy is that mRNA and protein analyses were performed from cells collected (or fixed) at different passages, 3 and 5, respectively. This may be important to consider as primary BMVECs are known to gradually lose their brain endothelial characteristics with cell passages and divisions, returning to a less specific endothelial state according to a "dedifferentiation" process. This can lead to an important loss of tightness and expression of specific BBB markers including tight junction proteins such as Claudin-5 and Occludin while maintaining their overall endothelial phenotype.[87,88] For Pr-2-derived cells, the discrepancies we observed in CLDN-5 mRNA and protein expressions remain unexplained. Noteworthy, contrary to previous reports showing a very well-organized CLDN-5 staining at the cell junctions of Pr-2 derived cells,[34,35] our data showed a disorganized expression of CLDN-5 in the cells we generated with the same protocol.

Some reports have already pointed out drawbacks regarding the phenotype of cells derived from the protocol of Lippmann and collaborators. For instance, Delsing et al. reported that these cells may exhibit a mixed endothelial and epithelial phenotype while Vatine and collaborators indicated that they share similarities with epithelial cells.[55,65] Another study mainly based on single-cell RNA sequencing and bioinformatic analysis reported that the protocol of Lippmann and collaborators generates $EPCAM^{+}/PECAM1^{-}$ neuro-ectodermal epithelial cells lacking endothelial identity.[67] In addition, it has been shown that Pr-2-derived cells lack expression of several key adhesion molecules precluding the use of these cells to study immune cell interactions with the BBB.[89] These reports recently led Lippmann and collaborators to rename these cells as "BMEC-like cells" to indicate that Pr-2-derived cells are not identical to human BMECs in vivo and therefore may not be appropriate for all applications.[85] Nevertheless, these cells are still referred to as brain ECs. Two observations appear to support this appellation.

First, like others, we also showed that Pr-2-derived cells expressed key BBB markers including tight junction proteins such as ZO-1 and Occludin but also efflux pump transporters. However, except for the loss of Claudin 5 expression in Pr-2-derived cells, we noted that BBB-specific markers were already expressed in undifferentiated hiPSCs with no major changes upon differentiation with Pr-2. Notably, ZO-1 and Occludin appeared to be expressed in a very similar pattern in undifferentiated iPSCs and Pr-2-derived cells, revealing extremely similar cobblestone-like shapes before and after differentiation. This common cellular morphology with very sharp edges at the intercellular junctions resembles honeycomb structures and is closer to that usually observed in epithelial cells rather than in BMVECs.[90] Hence, our observations are in line with previous reports showing that undifferentiated iPSCs exhibit an epithelial phenotype resulting from a mesenchymal-to-epithelial transition during the reprogramming process.[91,92] This seems to indicate that some key BBB features observed in Pr-2-derived cells and associated with an epithelial phenotype are not necessarily induced by Pr-2 but rather maintained during their differentiation. Taken together, our data confirm further the importance of distinguishing barrier properties from the endothelial phenotype, though not exclusive. This goes in line with the work from Lippmann and collaborators who reported barrier properties without endothelial features from Pr-2 derived cells.[85] Of note, epithelial cell lines such as Caco-2 or MDCK have already been used as BBB models displaying key barrier properties without showing endothelial features.[9]

Second, our data confirm the original and following reports showing that cells obtained with the Pr-2 method displayed solid barrier properties at the functional level including a similar penetration profile of small molecules to in vivo BBB, a P-GP efflux ability and the alteration of the functional integrity in response to TNF-α. Although these functions are not specific to the BBB and have also been observed on EpCs such as Caco-2,[9,93,94] they probably explain why this method has been used extensively. In particular, different reports using this differentiation protocol demonstrated good correlations between in vitro and in vivo barrier permeability of standard molecules known to display different, in vivo brain penetration.[34,42,46–48] This has led several groups to use this model as a tool to predict barrier permeability of small compounds or larger biomolecules with therapeutic interest.[95–98] Although the Pr-2 model generates cells endowed with EpC rather than EC features, it may be relevant to test molecules that cross barriers via cellular mechanisms shared by BMVECs and EpCs.[9] However, it may not be appropriate for mechanistic studies on the transport of molecules across HBMVECs or to study other mechanisms such as

immune cell interactions at the BBB.[89] This comparison led to unexpected results concerning the phenotype of the Pr-2-derived cells, raising concerns regarding their use for hiPSC-based BBB models.

4.2 | Pr-1-derived cells show EC features but form barrier models with low TEER

We compared the differentiation and barrier properties of hiPSCs generated by Pr-2 and Pr-1. The latter is based on a chemically defined method with mesodermal induction that is conceptually optimal from a developmental perspective. We selected the protocol published by Patsch et al., which describes the efficient and rapid conversion of PSCs into ECs with an efficiency exceeding 80% within 6 days of differentiation.[23] The procedure[71] was easily reproduced in our hands with two slight modifications. First, we replaced the mTSeR™1 medium used to culture the undifferentiated hiPSCs by the StemMACS iPS-Brew medium. Second, at the end of the differentiation process, we replaced the CD144 antibody by a CD34 antibody to improve the yield of magnetic cell sorting (not shown), a strategy that has already been used in similar differentiation protocols.[21,22,32] As expected, we produced from three different hiPSCs lines pure EC populations with high efficiency and reproducibility. Contrary to the Pr-2 procedure, Pr-1-derived cells displayed a full EC phenotype including the expression of all major EC markers, formed vascular tubes in vitro, and demonstrated uptake of acetylated LDL similarly to primary ECs (HBMVECs and HUVECs) used as controls. In comparison with HUVECs, Pr-1-derived cells displayed higher CD34 expression (both at the protein and mRNA levels), but this marker is known to be downregulated in primary HUVECs after several passages.[99] Also, even though we did not verify this point in the present study, it has been shown that Pr-1-derived cells form vascular structures in vivo after transplantation, which validates their angiogenic potential.[23] To our knowledge, this ability has never been demonstrated for Pr-2-derived cells and recently Lu and collaborators reported that these cells do not form lumenized vessels in immunocompromised mice.[67]

However, as previously reported by Patsch and colleagues, we found that the Pr-1 procedure does not appear to generate ECs with brain specialization (BMVECs). Thus, although we obtained homogeneous monolayers of contiguous cells (Figures 1 and 4), we showed that Pr-1-derived cells exhibit poor barrier properties including low TEER values. These values were close to those previously described for hiPSCs-derived ECs produced with the same or other chemically defined strategies, indicating that these hiPSC-ECs are close to peripheral ECs displaying low TEER such as HUVECs.[22,23,32] We also observed no or weak expression of key BBB markers such as Occludin and P-GP.

To improve the barrier properties of these "unspecified / naïve" cells, we tested different strategies aiming at reproducing a cerebral environment based either on co-cultures with cerebral cells (neural progenitors, glial cells, brain pericytes) or on cultures with molecules known to promote BMVEC specification: angiopoietin-1, Wnt-3a, TGFβ1, sonic hedgehog, retinoic acid, adrenomedullin, and cyclic AMP activators. However, there was no significant improvement in Pr-1 barrier properties (not shown). Consequently, we considered that in our experimental conditions, the cells generated using Pr-1 are not suitable for transport experiments of small or large molecules. Overall, our results were consistent with previous studies based on chemically defined methods that showed insufficient barrier properties[15,32,33,89] considering that a relevant in vitro BBB model should exhibit TEER values of at least 150–200 $\Omega.cm^2$ for transport experiments as previously reported.[6,80]

New differentiating methods are thus needed to specify hiPSC-derived ECs or hiPSC-derived vascular progenitors[21] towards a BMVEC phenotype optimal for BBB modeling. This will probably require a better understanding of the cellular and molecular mechanisms, including signaling pathways that occur during the specification of ECs in the developing brain. Recently, by comparing the transcriptomic profile of non- and CNS-derived murine ECs[100] or by performing a compound library screening on a CLDN5-GFP PSC line,[101] Roudnicky and collaborators identified new factors that control barrier resistance in ECs and showed a moderate improvement of the barrier properties in Pr-1-derived cells. Considering that the cerebral microenvironment made of and controlled by NVU cells is probably key to BMVEC specification and maintenance,[82,83] another way to improve the cerebral phenotype of hiPSC-derived ECs could be to more closely mimic the complexity of the cerebrovascular interface in vitro. Considerable efforts are currently being made to develop "mini brains" with 3D cytoarchitecture such as brain organoids, spheroids, or "brain-on-a-chip" whose interest goes beyond the simple modeling of the BBB.[102] Human iPS cells, through their ability to differentiate into different NVU cells, have an important role to play in the development of these innovative technologies. Recently, brain organoids produced from hiPSCs have been vascularized by hiPSC-derived ECs generated with a chemically-defined procedure close to the Pr-1 protocol.[103] Other strategies such as the supplementation of VEGF in the differentiation medium[104] or the ectopic induction of the expression of specific ETS transcription factors[105] have been used to induce the co-differentiation of ECs and the

vascularization of brain organoids. Further studies will determine whether these new technological developments will not only help to better understand neurovascular interactions but will also allow the establishment of reliable human BBB models.[106]

In conclusion, using different approaches and relevant cellular controls, we demonstrated that cells obtained with the Pr-2 differentiation procedure require further characterization. They display an epithelial rather than endothelial phenotype and our observations are supported by transcriptomic data from several studies. However, cells derived from this procedure may be of great value in some cases, especially due to their barrier properties including the expression of BBB transporter. As an alternative, cells generated by the Pr-1 procedure display EC features but lack the full differentiation into BMVECs yielding in vitro models with poor barrier properties and consequently currently unsuitable for BBB studies.

AUTHOR CONTRIBUTIONS

Stéphane D. Girard designed and performed experiments, analyzed data, and drafted the manuscript. Ingrid Julien-Gau, Yves Molino, and Benjamin F. Combes helped to perform experiments. Louise Greetham was involved in cell culture procedures. Michel Khrestchatisky and Emmanuel Nivet led the conception, supervised the project, and wrote the manuscript.

ACKNOWLEDGMENTS

We thank Françoise Jabès for her technical support regarding the in vitro BBB experiments and Guillaume Jacquot for his help concerning the analysis of small molecule permeability. This work was in part supported by funding from the Centre National de la Recherche Scientifique (CNRS) and Aix-Marseille Université, and by a public grant from the French National Research Agency (ANR, project "NANOVECTOR", ANR-15-CE18-0010). This work has received support from the French government under the Programme Investissements d'Avenir, Initiative d'Excellence d'Aix-Marseille Université via A*Midex (AMX-19-IET-004) and ANR (ANR-17-EURE-0029) funding.

DISCLOSURES

M.K. is the director of the UMR7051 Laboratory, and co-founder, shareholder, and scientific counsel of the Vect-Horus biotechnology company. The remaining authors declare no conflicts of interest.

DATA AVAILABILITY STATEMENT

No new datasets were generated during the current study. However, some data reported in the current study were derived from the following resources (GEO accession numbers: GSE97575, GSE97100, GSE97324, GSE108012, GSE129290, GSE 107898, GSE94935, GSE93511, and GSE111839) as reported in this article.

ORCID

Emmanuel Nivet https://orcid.org/0000-0001-7903-4059

REFERENCES

1. Abbott NJ, Patabendige AA, Dolman DE, Yusof SR, Begley DJ. Structure and function of the blood-brain barrier. *Neurobiol Dis*. 2010;37(1):13-25. doi:10.1016/j.nbd.2009.07.030
2. Aday S, Cecchelli R, Hallier-Vanuxeem D, Dehouck MP, Ferreira L. Stem cell-based human blood-brain barrier models for drug discovery and delivery. *Trends Biotechnol*. 2016;34(5):382-393. doi:10.1016/j.tibtech.2016.01.001
3. Larsen JM, Martin DR, Byrne ME. Recent advances in delivery through the blood-brain barrier. *Curr Top Med Chem*. 2014;14(9):1148-1160. doi:10.2174/1568026614666140329230311
4. Sweeney MD, Sagare AP, Zlokovic BV. Blood-brain barrier breakdown in Alzheimer disease and other neurodegenerative disorders. *Nat Rev Neurol*. 2018;14(3):133-150. doi:10.1038/nrneurol.2017.188
5. Patel MM, Patel BM. Crossing the blood-brain barrier: recent advances in drug delivery to the brain. *CNS Drugs*. 2017;31(2):109-133. doi:10.1007/s40263-016-0405-9
6. Wolff A, Antfolk M, Brodin B, Tenje M. In vitro blood-brain barrier models-an overview of established models and new microfluidic approaches. *J Pharm Sci*. 2015;104(9):2727-2746. doi:10.1002/jps.24329
7. Helms HC, Abbott NJ, Burek M, et al. In vitro models of the blood-brain barrier: an overview of commonly used brain endothelial cell culture models and guidelines for their use. *J Cereb Blood Flow Metab*. 2016;36(5):862-890. doi:10.1177/0271678X16630991
8. Neuhaus W. In vitro models of the blood-brain barrier. *Handb Exp Pharmacol*. 2021;265:75-110. doi:10.1007/164_2020_370
9. Hellinger E, Veszelka S, Toth AE, et al. Comparison of brain capillary endothelial cell-based and epithelial (MDCK-MDR1, Caco-2, and VB-Caco-2) cell-based surrogate blood-brain barrier penetration models. *Eur J Pharm Biopharm*. 2012;82(2):340-351. doi:10.1016/j.ejpb.2012.07.020
10. Veszelka S, Toth A, Walter FR, et al. Comparison of a rat primary cell-based blood-brain barrier model with epithelial and brain endothelial cell lines: gene expression and drug transport. *Front Mol Neurosci*. 2018;11:166. doi:10.3389/fnmol.2018.00166
11. Lundquist S, Renftel M, Brillault J, Fenart L, Cecchelli R, Dehouck MP. Prediction of drug transport through the blood-brain barrier in vivo: a comparison between two in vitro cell models. *Pharm Res*. 2002;19(7):976-981. doi:10.1023/a:1016462205267
12. Garberg P, Ball M, Borg N, et al. In vitro models for the blood-brain barrier. *Toxicol In Vitro*. 2005;19(3):299-334. doi:10.1016/j.tiv.2004.06.011
13. Boyer-Di Ponio J, El-Ayoubi F, Glacial F, et al. Instruction of circulating endothelial progenitors in vitro towards specialized blood-brain barrier and arterial phenotypes. *PloS One*. 2014;9(1):e84179. doi:10.1371/journal.pone.0084179

14. Cecchelli R, Aday S, Sevin E, et al. A stable and reproducible human blood-brain barrier model derived from hematopoietic stem cells. *PloS One*. 2014;9(6):e99733. doi:10.1371/journal.pone.0099733
15. Lauschke K, Frederiksen L, Hall VJ. Paving the way toward complex blood-brain barrier models using pluripotent stem cells. *Stem Cells Dev*. 2017;26(12):857-874. doi:10.1089/scd.2017.0003
16. Ferreira L. What human blood-brain barrier models can tell us about BBB function and drug discovery? *Expert Opin Drug Discovery*. 2019;14(11):1113-1123. doi:10.1080/17460441.2019.1646722
17. Appelt-Menzel A, Oerter S, Mathew S, et al. Human iPSC-derived blood-brain barrier models: valuable tools for preclinical drug discovery and development? *Curr Protoc Stem Cell Biol*. 2020;55(1):e122. doi:10.1002/cpsc.122
18. Lippmann ES, Al-Ahmad A, Palecek SP, Shusta EV. Modeling the blood-brain barrier using stem cell sources. *Fluids Barriers CNS*. 2013;10(1):2. doi:10.1186/2045-8118-10-2
19. Bosworth AM, Faley SL, Bellan LM, Lippmann ES. Modeling neurovascular disorders and therapeutic outcomes with human-induced pluripotent stem cells. *Front Bioeng Biotechnol*. 2017;5:87. doi:10.3389/fbioe.2017.00087
20. Logan S, Arzua T, Canfield SG, et al. Studying human neurological disorders using induced pluripotent stem cells: from 2D monolayer to 3D organoid and blood brain barrier models. *Compr Physiol*. 2019;9(2):565-611. doi:10.1002/cphy.c180025
21. Kurian L, Sancho-Martinez I, Nivet E, et al. Conversion of human fibroblasts to angioblast-like progenitor cells. *Nat Methods*. 2013;10(1):77-83. doi:10.1038/nmeth.2255
22. Lian X, Bao X, Al-Ahmad A, et al. Efficient differentiation of human pluripotent stem cells to endothelial progenitors via small-molecule activation of WNT signaling. *Stem Cell Reports*. 2014;3(5):804-816. doi:10.1016/j.stemcr.2014.09.005
23. Patsch C, Challet-Meylan L, Thoma EC, et al. Generation of vascular endothelial and smooth muscle cells from human pluripotent stem cells. *Nat Cell Biol*. 2015;17(8):994-1003. doi:10.1038/ncb3205
24. Liu X, Qi J, Xu X, Zeisberg M, Guan K, Zeisberg EM. Differentiation of functional endothelial cells from human induced pluripotent stem cells: a novel, highly efficient and cost effective method. *Differentiation*. 2016;92(4):225-236. doi:10.1016/j.diff.2016.05.004
25. Nguyen MTX, Okina E, Chai X, et al. Differentiation of human embryonic stem cells to endothelial progenitor cells on Laminins in defined and xeno-free systems. *Stem Cell Reports*. 2016;7(4):802-816. doi:10.1016/j.stemcr.2016.08.017
26. Lin Y, Gil CH, Yoder MC. Differentiation, evaluation, and application of human induced pluripotent stem cell-derived endothelial cells. *Arterioscler Thromb Vasc Biol*. 2017;37(11):2014-2025. doi:10.1161/ATVBAHA.117.309962
27. Belt H, Koponen JK, Kekarainen T, et al. Temporal dynamics of gene expression during endothelial cell differentiation from human iPS cells: a comparison study of Signalling factors and small molecules. *Front Cardiovasc Med*. 2018;5:16. doi:10.3389/fcvm.2018.00016
28. Halaidych OV, Freund C, van den Hil F, et al. Inflammatory responses and barrier function of endothelial cells derived from human induced pluripotent stem cells. *Stem Cell Reports*. 2018;10(5):1642-1656. doi:10.1016/j.stemcr.2018.03.012
29. Olmer R, Engels L, Usman A, et al. Differentiation of human pluripotent stem cells into functional endothelial cells in scalable suspension culture. *Stem Cell Reports*. 2018;10(5):1657-1672. doi:10.1016/j.stemcr.2018.03.017
30. Farkas S, Simara P, Rehakova D, Veverkova L, Koutna I. Endothelial progenitor cells produced from human pluripotent stem cells by a synergistic combination of cytokines, small compounds, and serum-free medium. *Front Cell Dev Biol*. 2020;8:309. doi:10.3389/fcell.2020.00309
31. Nishihara H, Gastfriend BD, Kasap P, Palecek SP, Shusta EV, Engelhardt B. Differentiation of human pluripotent stem cells to brain microvascular endothelial cell-like cells suitable to study immune cell interactions. *STAR Protocols*. 2021;2(2):100563. doi:10.1016/j.xpro.2021.100563
32. Minami H, Tashiro K, Okada A, et al. Generation of brain microvascular endothelial-like cells from human induced pluripotent stem cells by Co-culture with C6 glioma cells. *PloS One*. 2015;10(6):e0128890. doi:10.1371/journal.pone.0128890
33. Praca C, Rosa SC, Sevin E, Cecchelli R, Dehouck MP, Ferreira LS. Derivation of brain capillary-like endothelial cells from human pluripotent stem cell-derived endothelial progenitor cells. *Stem Cell Reports*. 2019;13(4):599-611. doi:10.1016/j.stemcr.2019.08.002
34. Lippmann ES, Azarin SM, Kay JE, et al. Derivation of blood-brain barrier endothelial cells from human pluripotent stem cells. *Nat Biotechnol*. 2012;30(8):783-791. doi:10.1038/nbt.2247
35. Lippmann ES, Al-Ahmad A, Azarin SM, Palecek SP, Shusta EV. A retinoic acid-enhanced, multicellular human blood-brain barrier model derived from stem cell sources. *Sci Rep*. 2014;4:4160. doi:10.1038/srep04160
36. Wilson HK, Canfield SG, Hjortness MK, Palecek SP, Shusta EV. Exploring the effects of cell seeding density on the differentiation of human pluripotent stem cells to brain microvascular endothelial cells. *Fluids Barriers CNS*. 2015;12:13. doi:10.1186/s12987-015-0007-9
37. Wilson HK, Faubion MG, Hjortness MK, Palecek SP, Shusta EV. Cryopreservation of brain endothelial cells derived from human induced pluripotent stem cells is enhanced by rho-associated coiled coil-containing kinase inhibition. *Tissue Eng Part C Methods*. 2016;22(12):1085-1094. doi:10.1089/ten.TEC.2016.0345
38. Hollmann EK, Bailey AK, Potharazu AV, Neely MD, Bowman AB, Lippmann ES. Accelerated differentiation of human induced pluripotent stem cells to blood-brain barrier endothelial cells. *Fluids Barriers CNS*. 2017;14(1):9. doi:10.1186/s12987-017-0059-0
39. Qian T, Maguire SE, Canfield SG, et al. Directed differentiation of human pluripotent stem cells to blood-brain barrier endothelial cells. *Sci Adv*. 2017;3(11):e1701679. doi:10.1126/sciadv.1701679
40. Neal EH, Marinelli NA, Shi Y, et al. A simplified, fully defined differentiation scheme for producing blood-brain barrier endothelial cells from human iPSCs. *Stem Cell Reports*. 2019;12(6):1380-1388. doi:10.1016/j.stemcr.2019.05.008
41. Katt ME, Xu ZS, Gerecht S, Searson PC. Human brain microvascular endothelial cells derived from the BC1 iPS cell line exhibit a blood-brain barrier phenotype. *PloS One*. 2016;11(4):e0152105. doi:10.1371/journal.pone.0152105
42. Mantle JL, Min L, Lee KH. Minimum Transendothelial electrical resistance thresholds for the study of small and large

molecule drug transport in a human in vitro blood-brain barrier model. *Mol Pharm*. 2016;13(12):4191-4198. doi:10.1021/acs.molpharmaceut.6b00818

43. Appelt-Menzel A, Cubukova A, Gunther K, et al. Establishment of a human blood-brain barrier Co-culture model mimicking the neurovascular unit using induced Pluri- and multipotent stem cells. *Stem Cell Reports*. 2017;8(4):894-906. doi:10.1016/j.stemcr.2017.02.021
44. Kokubu Y, Yamaguchi T, Kawabata K. In vitro model of cerebral ischemia by using brain microvascular endothelial cells derived from human induced pluripotent stem cells. *Biochem Biophys Res Commun*. 2017;486(2):577-583. doi:10.1016/j.bbrc.2017.03.092
45. Kurosawa T, Tega Y, Higuchi K, et al. Expression and functional characterization of drug transporters in brain microvascular endothelial cells derived from human induced pluripotent stem cells. *Mol Pharm*. 2018;15(12):5546-5555. doi:10.1021/acs.molpharmaceut.8b00697
46. Ribecco-Lutkiewicz M, Sodja C, Haukenfrers J, et al. A novel human induced pluripotent stem cell blood-brain barrier model: applicability to study antibody-triggered receptor-mediated transcytosis. *Sci Rep*. 2018;8(1):1873. doi:10.1038/s41598-018-19522-8
47. Ohshima M, Kamei S, Fushimi H, Mima S, Yamada T, Yamamoto T. Prediction of drug permeability using In vitro blood-brain barrier models with human induced pluripotent stem cell-derived brain microvascular endothelial cells. *Biores Open Access*. 2019;8(1):200-209. doi:10.1089/biores.2019.0026
48. Roux GL, Jarray R, Guyot AC, et al. Proof-of-concept study of drug brain permeability between in vivo human brain and an in vitro iPSCs-human blood-brain barrier model. *Sci Rep*. 2019;9(1):16310. doi:10.1038/s41598-019-52213-6
49. Neal EH, Katdare KA, Shi Y, Marinelli NA, Hagerla KA, Lippmann ES. Influence of basal media composition on barrier fidelity within human pluripotent stem cell-derived blood-brain barrier models. *J Neurochem*. 2021;159(6):980-991. doi:10.1111/jnc.15532
50. DeStefano JG, Xu ZS, Williams AJ, Yimam N, Searson PC. Effect of shear stress on iPSC-derived human brain microvascular endothelial cells (dhBMECs). *Fluids Barriers CNS*. 2017;14(1):20. doi:10.1186/s12987-017-0068-z
51. Wang YI, Abaci HE, Shuler ML. Microfluidic blood-brain barrier model provides in vivo-like barrier properties for drug permeability screening. *Biotechnol Bioeng*. 2017;114(1):184-194. doi:10.1002/bit.26045
52. Grifno GN, Farrell AM, Linville RM, et al. Tissue-engineered blood-brain barrier models via directed differentiation of human induced pluripotent stem cells. *Sci Rep*. 2019;9(1):13957. doi:10.1038/s41598-019-50193-1
53. Motallebnejad P, Thomas A, Swisher SL, Azarin SM. An isogenic hiPSC-derived BBB-on-a-chip. *Biomicrofluidics*. 2019;13(6):064119. doi:10.1063/1.5123476
54. Park TE, Mustafaoglu N, Herland A, et al. Hypoxia-enhanced blood-brain barrier Chip recapitulates human barrier function and shuttling of drugs and antibodies. *Nat Commun*. 2019;10(1):2621. doi:10.1038/s41467-019-10588-0
55. Vatine GD, Barrile R, Workman MJ, et al. Human iPSC-derived blood-brain barrier chips enable disease modeling and personalized medicine applications. *Cell Stem Cell*. 2019;24(6):995-1005.e6. doi:10.1016/j.stem.2019.05.011
56. Jagadeesan S, Workman MJ, Herland A, Svendsen CN, Vatine GD. Generation of a human iPSC-based blood-brain barrier Chip. *J Vis Exp*. 2020;(157). doi:10.3791/60925
57. Canfield SG, Stebbins MJ, Morales BS, et al. An isogenic blood-brain barrier model comprising brain endothelial cells, astrocytes, and neurons derived from human induced pluripotent stem cells. *J Neurochem*. 2017;140(6):874-888. doi:10.1111/jnc.13923
58. Canfield SG, Stebbins MJ, Faubion MG, Gastfriend BD, Palecek SP, Shusta EV. An isogenic neurovascular unit model comprised of human induced pluripotent stem cell-derived brain microvascular endothelial cells, pericytes, astrocytes, and neurons. *Fluids Barriers CNS*. 2019;16(1):25. doi:10.1186/s12987-019-0145-6
59. Blanchard JW, Bula M, Davila-Velderrain J, et al. Reconstruction of the human blood-brain barrier in vitro reveals a pathogenic mechanism of APOE4 in pericytes. *Nat Med*. 2020;26:952-963. doi:10.1038/s41591-020-0886-4
60. Lim RG, Quan C, Reyes-Ortiz AM, et al. Huntington's disease iPSC-derived brain microvascular endothelial cells reveal WNT-mediated Angiogenic and blood-brain barrier deficits. *Cell Rep*. 2017;19(7):1365-1377. doi:10.1016/j.celrep.2017.04.021
61. Vatine GD, Al-Ahmad A, Barriga BK, et al. Modeling psychomotor retardation using iPSCs from MCT8-deficient patients indicates a prominent role for the blood-brain barrier. *Cell Stem Cell*. 2017;20(6):831-843 e5. doi:10.1016/j.stem.2017.04.002
62. Lee CAA, Seo HS, Armien AG, Bates FS, Tolar J, Azarin SM. Modeling and rescue of defective blood-brain barrier function of induced brain microvascular endothelial cells from childhood cerebral adrenoleukodystrophy patients. *Fluids Barriers CNS*. 2018;15(1):9. doi:10.1186/s12987-018-0094-5
63. Oikari LE, Pandit R, Stewart R, et al. Altered brain endothelial cell phenotype from a familial Alzheimer mutation and its potential implications for amyloid clearance and drug delivery. *Stem Cell Reports*. 2020;14:924-939. doi:10.1016/j.stemcr.2020.03.011
64. Lu TM, Barcia Duran JG, Houghton S, Rafii S, Redmond D, Lis R. Human induced pluripotent stem cell-derived brain endothelial cells: current controversies. *Front Physiol*. 2021;12:642812. doi:10.3389/fphys.2021.642812
65. Delsing L, Donnes P, Sanchez J, et al. Barrier properties and transcriptome expression in human iPSC-derived models of the blood-brain barrier. *Stem Cells*. 2018;36(12):1816-1827. doi:10.1002/stem.2908
66. Linville RM, Sklar MB, Grifno GN, et al. Three-dimensional microenvironment regulates gene expression, function, and tight junction dynamics of iPSC-derived blood-brain barrier microvessels. *Fluids Barriers CNS*. 2022;19(1):87. doi:10.1186/s12987-022-00377-1
67. Lu TM, Houghton S, Magdeldin T, et al. Pluripotent stem cell-derived epithelium misidentified as brain microvascular endothelium requires ETS factors to acquire vascular fate. *Proc Natl Acad Sci U S A*. 2021;118(8):e2016950118. doi:10.1073/pnas.2016950118
68. Aasen T, Raya A, Barrero MJ, et al. Efficient and rapid generation of induced pluripotent stem cells from human keratinocytes. *Nat Biotechnol*. 2008;26(11):1276-1284. doi:10.1038/nbt.1503
69. Xia Y, Nivet E, Sancho-Martinez I, et al. Directed differentiation of human pluripotent cells to ureteric bud kidney progenitor-like cells. *Nat Cell Biol*. 2013;15(12):1507-1515. doi:10.1038/ncb2872

70. Yu J, Vodyanik MA, Smuga-Otto K, et al. Induced pluripotent stem cell lines derived from human somatic cells. *Science*. 2007;318(5858):1917-1920. doi:10.1126/science.1151526
71. Challet Meylan L, Patsch C, Thoma E. Endothelial cells differentiation from hPSCs. *Protocol Exchange*. 2015. doi:10.1038/protex.2015.055
72. Molino Y, Jabes F, Lacassagne E, Gaudin N, Khrestchatisky M. Setting-up an in vitro model of rat blood-brain barrier (BBB): a focus on BBB impermeability and receptor-mediated transport. *J Vis Exp*. 2014;88:e51278. doi:10.3791/51278
73. Stebbins MJ, Wilson HK, Canfield SG, Qian T, Palecek SP, Shusta EV. Differentiation and characterization of human pluripotent stem cell-derived brain microvascular endothelial cells. *Methods*. 2016;101:93-102. doi:10.1016/j.ymeth.2015.10.016
74. Beillard E, Pallisgaard N, van der Velden VH, et al. Evaluation of candidate control genes for diagnosis and residual disease detection in leukemic patients using 'real-time' quantitative reverse-transcriptase polymerase chain reaction (RQ-PCR) - a Europe against cancer program. *Leukemia*. 2003;17(12):2474-2486. doi:10.1038/sj.leu.2403136
75. Voyta JC, Via DP, Butterfield CE, Zetter BR. Identification and isolation of endothelial cells based on their increased uptake of acetylated-low density lipoprotein. *J Cell Biol*. 1984;99(6):2034-2040. doi:10.1083/jcb.99.6.2034
76. Landry ML, Foxman EF. Antiviral response in the nasopharynx identifies patients with respiratory virus infection. *J Infect Dis*. 2018;217(6):897-905. doi:10.1093/infdis/jix648
77. Lickwar CR, Camp JG, Weiser M, et al. Genomic dissection of conserved transcriptional regulation in intestinal epithelial cells. *PLoS Biol*. 2017;15(8):e2002054. doi:10.1371/journal.pbio.2002054
78. Zhang J, Schwartz MP, Hou Z, et al. A genome-wide analysis of human pluripotent stem cell-derived endothelial cells in 2D or 3D culture. *Stem Cell Reports*. 2017;8(4):907-918. doi:10.1016/j.stemcr.2017.02.014
79. Sabbagh MF, Heng JS, Luo C, et al. Transcriptional and epigenomic landscapes of CNS and non-CNS vascular endothelial cells. *Elife*. 2018;7:e36187. doi:10.7554/eLife.36187
80. Reichel A, Begley DJ, Abbott NJ. An overview of in vitro techniques for blood-brain barrier studies. *Methods Mol Med*. 2003;89:307-324. doi:10.1385/1-59259-419-0:307
81. Srinivasan B, Kolli AR, Esch MB, Abaci HE, Shuler ML, Hickman JJ. TEER measurement techniques for in vitro barrier model systems. *J Lab Autom*. 2015;20(2):107-126. doi:10.1177/2211068214561025
82. Engelhardt B. Development of the blood-brain barrier. *Cell Tissue Res*. 2003;314(1):119-129. doi:10.1007/s00441-003-0751-z
83. Obermeier B, Daneman R, Ransohoff RM. Development, maintenance and disruption of the blood-brain barrier. *Nat Med*. 2013;19(12):1584-1596. doi:10.1038/nm.3407
84. Kurz H. Cell lineages and early patterns of embryonic CNS vascularization. *Cell Adh Migr*. 2009;3(2):205-210.
85. Lippmann ES, Azarin SM, Palecek SP, Shusta EV. Commentary on human pluripotent stem cell-based blood-brain barrier models. *Fluids Barriers CNS*. 2020;17(1):64. doi:10.1186/s12987-020-00222-3
86. Daneman R, Zhou L, Agalliu D, Cahoy JD, Kaushal A, Barres BA. The mouse blood-brain barrier transcriptome: a new resource for understanding the development and function of brain endothelial cells. *PloS One*. 2010;5(10):e13741. doi:10.1371/journal.pone.0013741
87. Fujimoto T, Morofuji Y, Nakagawa S, et al. Comparison of the rate of dedifferentiation with increasing passages among cell sources for an in vitro model of the blood-brain barrier. *J Neural Transm*. 2020;127(8):1117-1124. doi:10.1007/s00702-020-02202-1
88. Sabbagh MF, Nathans J. A genome-wide view of the de-differentiation of central nervous system endothelial cells in culture. *Elife*. 2020;9:e51276. doi:10.7554/eLife.51276
89. Nishihara H, Gastfriend BD, Soldati S, et al. Advancing human induced pluripotent stem cell-derived blood-brain barrier models for studying immune cell interactions. *FASEB J*. 2020;34:16693-16715. doi:10.1096/fj.202001507RR
90. Wang CC, Jamal L, Janes KA. Normal morphogenesis of epithelial tissues and progression of epithelial tumors. *Wiley Interdiscip Rev Syst Biol Med*. 2012;4(1):51-78. doi:10.1002/wsbm.159
91. Li R, Liang J, Ni S, et al. A mesenchymal-to-epithelial transition initiates and is required for the nuclear reprogramming of mouse fibroblasts. *Cell Stem Cell*. 2010;7(1):51-63. doi:10.1016/j.stem.2010.04.014
92. Teshigawara R, Cho J, Kameda M, Tada T. Mechanism of human somatic reprogramming to iPS cell. *Lab Invest*. 2017;97(10):1152-1157. doi:10.1038/labinvest.2017.56
93. Hano M, Tomasova L, Seres M, Pavlikova L, Breier A, Sulova Z. Interplay between P-glycoprotein expression and resistance to endoplasmic reticulum stressors. *Molecules*. 2018;23(2):337. doi:10.3390/molecules23020337
94. Ma TY, Iwamoto GK, Hoa NT, et al. TNF-alpha-induced increase in intestinal epithelial tight junction permeability requires NF-kappa B activation. *Am J Physiol Gastrointest Liver Physiol*. 2004;286(3):G367-G376. doi:10.1152/ajpgi.00173.2003
95. Clark PA, Al-Ahmad AJ, Qian T, et al. Analysis of cancer-targeting Alkylphosphocholine analogue permeability characteristics using a human induced pluripotent stem cell blood-brain barrier model. *Mol Pharm*. 2016;13(9):3341-3349. doi:10.1021/acs.molpharmaceut.6b00441
96. Gallagher E, Minn I, Chambers JE, Searson PC. In vitro characterization of pralidoxime transport and acetylcholinesterase reactivation across MDCK cells and stem cell-derived human brain microvascular endothelial cells (BC1-hBMECs). *Fluids Barriers CNS*. 2016;13(1):10. doi:10.1186/s12987-016-0035-0
97. Chiou B, Neal EH, Bowman AB, Lippmann ES, Simpson IA, Connor JR. Pharmaceutical iron formulations do not cross a model of the human blood-brain barrier. *PloS One*. 2018;13(6):e0198775. doi:10.1371/journal.pone.0198775
98. Mantle JL, Lee KH. Immunoglobulin G transport increases in an in vitro blood-brain barrier model with amyloid-beta and with neuroinflammatory cytokines. *Biotechnol Bioeng*. 2019;116(7):1752-1761. doi:10.1002/bit.26967
99. Fina L, Molgaard HV, Robertson D, et al. Expression of the CD34 gene in vascular endothelial cells. *Blood*. 1990;75(12):2417-2426.
100. Roudnicky F, Kim BK, Lan Y, et al. Identification of a combination of transcription factors that synergistically increases endothelial cell barrier resistance. *Sci Rep*. 2020;10(1):3886. doi:10.1038/s41598-020-60688-x
101. Roudnicky F, Zhang JD, Kim BK, et al. Inducers of the endothelial cell barrier identified through chemogenomic screening in genome-edited hPSC-endothelial cells. *Proc Natl Acad Sci U S A*. 2020;117(33):19854-19865. doi:10.1073/pnas.1911532117

102. Bhalerao A, Sivandzade F, Archie SR, Chowdhury EA, Noorani B, Cucullo L. In vitro modeling of the neurovascular unit: advances in the field. *Fluids Barriers CNS*. 2020;17(1):22. doi:10.1186/s12987-020-00183-7
103. Pham MT, Pollock KM, Rose MD, et al. Generation of human vascularized brain organoids. *Neuroreport*. 2018;29(7):588-593. doi:10.1097/WNR.0000000000001014
104. Ham O, Jin YB, Kim J, Lee MO. Blood vessel formation in cerebral organoids formed from human embryonic stem cells. *Biochem Biophys Res Commun*. 2020;521(1):84-90. doi:10.1016/j.bbrc.2019.10.079
105. Cakir B, Xiang Y, Tanaka Y, et al. Engineering of human brain organoids with a functional vascular-like system. *Nat Methods*. 2019;16(11):1169-1175. doi:10.1038/s41592-019-0586-5
106. Waldau B. Using miniature brain implants in rodents for novel drug discovery. *Expert Opin Drug Discovery*. 2019;14(4):379-386. doi:10.1080/17460441.2019.1577816

SUPPORTING INFORMATION

Additional supporting information can be found online in the Supporting Information section at the end of this article.

How to cite this article: Girard SD, Julien-Gau I, Molino Y, et al. High and low permeability of human pluripotent stem cell–derived blood–brain barrier models depend on epithelial or endothelial features. *The FASEB Journal*. 2023;37:e22770. doi:10.1096/fj.202201422R